





UHMK1 promotes gastric cancer progression through reprogramming nucleotide metabolism

Xing Feng^{1,2,†} , Dong Ma^{3,†}, Jiabao Zhao^{4,†}, Yongxi Song^{5,†}, Yuekun Zhu^{6,7}, Qingxin Zhou⁸, Fei Ma⁹, Xing Liu¹⁰, Mengya Zhong⁴, Yu Liu⁴, Yubo Xiong⁴, Xingfeng Qiu⁴, Zhen Zhang¹¹, Heng Zhang¹², Yongxiang Zhao¹³, Kaiguang Zhang^{14,*} , Xuehui Hong^{4,†,**,††}  & Zhiyong Zhang^{1,15,‡,***} 

Abstract

UHMK1 is a nuclear serine/threonine kinase recently implicated in carcinogenesis. However, the functions and action mechanisms of UHMK1 in the pathogenesis of human gastric cancer (GC) are unclear. Here, we observed that UHMK1 was markedly upregulated in GC. UHMK1 silencing strongly inhibited GC aggressiveness. Interestingly, UHMK1-induced GC progression was mediated primarily via enhancing *de novo* purine synthesis because inhibiting purine synthesis reversed the effects of UHMK1 overexpression. Mechanistically, UHMK1 activated ATF4, an important transcription factor in nucleotide synthesis, by phosphorylating NCOA3 at Ser (S) 1062 and Thr (T) 1067. This event significantly enhanced the binding of NCOA3 to ATF4 and the expression of purine metabolism-associated target genes. Conversely, deficient phosphorylation of NCOA3 at S1062/T1067 significantly abrogated the function of UHMK1 in GC development. Clinically, *Helicobacter pylori* and GC-associated UHMK1 mutation induced NCOA3-S1062/T1067 phosphorylation and enhanced the activity of ATF4 and UHMK1. Importantly, the level of UHMK1 was significantly correlated with the level of phospho-NCOA3 (S1062/T1067) in human GC specimens. Collectively, these results show that the UHMK1-activated *de novo* purine synthesis pathway significantly promotes GC development.

Keywords ATF4; gastric cancer; NCOA3; purine metabolism; UHMK1

Subject Categories Cancer; Metabolism

DOI 10.15252/emboj.2019102541 | Received 27 May 2019 | Revised 2 December 2019 | Accepted 6 December 2019 | Published online 23 January 2020

The EMBO Journal (2020) 39: e102541

Introduction

Gastric cancer (GC) has been indicated to be one of the deadliest malignancies. *Helicobacter pylori* (*H. pylori*) infection, dietary habits, and other environmental risk agents contribute greatly to GC development (Wroblewski *et al*, 2010). Although surgical resection is a primary therapeutic option for GC patients, the 5-year survival rate remains approximately 30.6% but is only 5.2% for patients with advanced stages (Yusefi *et al*, 2018). Therefore, a better understanding of molecular aberrations involved in GC pathogenesis is necessary to improve the clinical outcomes of GC patients.

U2AF homology motif kinase 1 (UHMK1) is a ubiquitously expressed nuclear serine (Ser, S)/threonine (Thr, T) kinase (Franccone *et al*, 2010). It was initially identified to regulate the function of stathmin (Barbutti *et al*, 2017). Since then, UHMK1 has been indicated to bind a range of proteins, such as eEF1A, FAM64, cyclin-dependent kinase inhibitor (CDKI), p27^{KIP1}, SF3b155, and CPEB1, suggesting the varied roles of UHMK1 in different cellular processes (Manceau *et al*, 2008; Cambray *et al*, 2009). Although UHMK1 dysregulation or mutation has been recently indicated to be a high-

1 The Affiliated Hospital of Guilin Medical University, Guangxi Key Laboratory of Brain and Cognitive Neuroscience, Guangxi Neurological Diseases Clinical Research Center, Guilin, Guangxi, China

2 Department of Immunobiology, Yale University School of Medicine, New Haven, CT, USA

3 Guangdong Provincial People's Hospital, Guangdong Academy of Medical Sciences, Guangzhou, China

4 Department of Gastrointestinal Surgery, Zhongshan Hospital, School of Medicine, Xiamen University, Xiamen, China

5 Department of Surgical Oncology and General Surgery, The First Hospital of China Medical University, Shenyang, China

6 Medical Center, Duke University, Durham, NC, USA

7 Department of General Surgery, The First Affiliated Hospital of Harbin Medical University, Harbin, China

8 Department of Oncology, The Third Affiliated Hospital of Harbin Medical University, Harbin, China

9 Department of General Surgery, The Second Affiliated Hospital of Harbin Medical University, Harbin, China

10 Department of Neurosurgery, Beijing Tiantan Hospital, Capital Medical University, Beijing, China

11 Department of General Surgery, The First Affiliated Hospital of Anhui Medical University, Anhui, China

12 Department of Histology and Embryology, Xiang Ya School of Medicine, Central South University, Changsha, China

13 National Center for International Research of Biological Targeting Diagnosis and Therapy (Guangxi Key Laboratory of Biological Targeting Diagnosis and Therapy Research), Guangxi Medical University, Nanning, China

14 Department of Digestive Disease, The First Affiliated Hospital of USTC, Anhui Provincial Hospital, University of Science and Technology of China, Anhui, China

15 Department of Surgery, Robert-Wood-Johnson Medical School University Hospital, Rutgers University, The State University of New Jersey, New Brunswick, NJ, USA

*Corresponding author. Tel: +86 551 62283114; Fax: +86 551 62283114; E-mail: zhangkaiguang@ustc.edu.cn

**Corresponding author. Tel: +86 592 2993182; Fax: +86 592 2993182; E-mails: hongxu@xmu.edu.cn; hxh5717@163.com

***Corresponding author. Tel: +1 732 2356853; Fax: +1 732 2356853; E-mails: zhangz2@rwjms.rutgers.edu; zhiyongzhng3@gmail.com

†These authors contributed equally to this work

‡These authors contributed equally to this work as senior authors

penetrant factor in different types of human tumors, such as pancreatic and ovarian cancer (Katchman *et al*, 2017; Grant *et al*, 2018; Wang *et al*, 2018), its effect and action mechanisms in most cancers including GC still were uncovered.

Tumor cells reprogram glucose metabolism by switching from oxidative phosphorylation (OXPHOS) to a process termed the Warburg effect (Song *et al*, 2014). However, emerging evidence indicates that dysregulated purine metabolism is implicated in tumors (Nishimura *et al*, 2019). This finding is not surprising, because many metabolites from the Warburg effect or pentose phosphate pathway (PPP) are essential carbon sources for purine biosynthesis (Hong *et al*, 2014). Several kinases and transcription factors (TFs), for example, mechanistic target of rapamycin kinase (mTOR), activating transcription factor 4 (ATF4), microphthalmia-associated transcription factor (MITF), and c-Myc, dictate cancer-dependent purine biosynthesis (Ben-Sahra *et al*, 2016; Karigane *et al*, 2016). We recently reported that dual-specificity tyrosine-(Y)-phosphorylation-regulated kinase 3 (Dyrk3) inhibited liver cancer by downregulating purine synthesis (Ma *et al*, 2019). However, the effect of purine metabolism on GC is not clear.

Herein, by analyzing data from The Cancer Genome Atlas (TCGA) and Oncomine database, we found that genomic DNA of UHMK1 was frequently amplified in GC. Therefore, we further investigated the role and mechanism of UHMK1 in GC. We found that upregulation of UHMK1 suggested poor prognosis of GC patients. We demonstrated that UHMK1 functioned as an oncogene mainly by promoting the purine synthesis pathway in GC. Therefore, UHMK1-enhanced nucleotide synthesis might be an important therapeutic target in GC.

Results

High-level UHMK1 expression is strongly correlated with GC aggressiveness

We first examined the functions of UHMK1 in GC by investigating the relative levels of UHMK1 in five paired GC patient tissues and corresponding normal tissues. The amount of UHMK1 was significantly increased in GC tissues compared with control tissues (Fig 1A). In addition, the amount of UHMK1 in most GC cell lines was often higher than that in the GES-1 cell line, a normal gastric epithelial cell line (Fig 1B). Similar results were found in other

studies of GC in TCGA and Oncomine datasets (Fig EV1A–F). The tissue array analysis results indicated that compared to normal tissues, GC tissues presented increased expression levels of UHMK1 (Fig 1C) and that the percentage of cells with UHMK1 expression in patients with stage I, II, III, and IV GC was 18.2, 36.4, 69, and 100, respectively (Fig 1D), further implying that the level of UHMK1 is strongly correlated with GC malignancy. Analysis of 100 patients with GC confirmed that the level of UHMK1 was strongly associated with tumor status, stage, and lymph node metastasis (Fig 1E and Appendix Table S1). Kaplan–Meier analysis of two independent cohorts indicated that GC patients with higher amounts of UHMK1 presented shorter disease-free survival (DFS) and overall survival (OS) times (Figs 1F and EV1G and H). Multivariate analyses identified UHMK1 as an independent prognostic factor in GC (Appendix Table S2). Collectively, our data reveal that UHMK1 may promote the pathogenesis of GC.

UHMK1 knockdown strongly inhibits the proliferation and invasion of GC cells, possibly via metabolic pathway reprogramming

To elucidate the functions of UHMK1 in GC, three lentivirus-mediated UHMK1-specific short hairpin RNAs (shRNAs) were transfected to knock down endogenous UHMK1 in two GC cell lines. shUHMK1-#1 and shUHMK1-#2, with high inhibition rates, were selected for further experiments (Fig 2A). UHMK1 deficiency significantly reduced GC cell proliferation, colony formation, migration, and invasion relative to the corresponding levels in negative control cells (Figs 2B and C, and EV2A–F). However, reintroduction of a shRNA-resistant UHMK1 construct, UHMK1Δ, significantly reversed these phenotypes in SGC7901-shUHMK1-#1 or MGC803-shUHMK1-#1 cells (Figs 2B and C, and EV2A–F). Consistent with this result, UHMK1 overexpression in BGC823 and HGC27 cells markedly promoted their proliferative and invasive abilities (Fig EV2G–M).

In vivo, knockdown of UHMK1 significantly decreased GC tumorigenesis and the number of abdominal metastatic nodules compared to these parameters in control mice (Fig 2D–F). However, UHMK1 overexpression significantly promoted GC growth and increased the number of metastatic nodules (Figs EV2N and 2G).

To further uncover the function of UHMK1 in GC, we assessed the transcriptomes of GC patients in TCGA with varying levels of UHMK1 expression. And the top 500 differentially expressed genes were analyzed in UHMK1^{high} versus UHMK1^{low} patients

Figure 1. High expression of UHMK1 predicts poor prognosis of GC patients.

- A UHMK1 levels in tumor tissues (T) and corresponding nontumor tissues (N) from five GC patients were analyzed using Western blotting and qRT-PCR. The relative mRNA expression of UHMK1 was presented as mean \pm standard deviation from three replicates. Pairwise two-tailed statistical significance was assessed by Student's *t*-test.
- B Immunoblotting and qRT-PCR were used to measure the levels of UHMK1 in GES-1 and GC cell lines. The relative mRNA expression of UHMK1 was presented as mean \pm standard deviation from three replicates. Pairwise two-tailed statistical significance was assessed by Student's *t*-test.
- C IHC analysis of UHMK1 expression in a GC patient tissue array ($n = 102$). Representative images are shown. Scale bars = 100 μ m.
- D The IHC signals were scored using the Allred score as described in Material and Methods. Data were shown as mean \pm standard deviation from three independent experiments.
- E UHMK1 expression in 100 GC patients was analyzed based on the following parameters: tumor stage, tumor status, and lymph node invasion status. Fisher's test was applied to calculate the exact *P* value.
- F Patients with GC were stratified by the UHMK1 level ($n = 100$); OS and DFS were assessed by Kaplan–Meier analysis.
- Data information: **P* < 0.05, ***P* < 0.01, ****P* < 0.001.

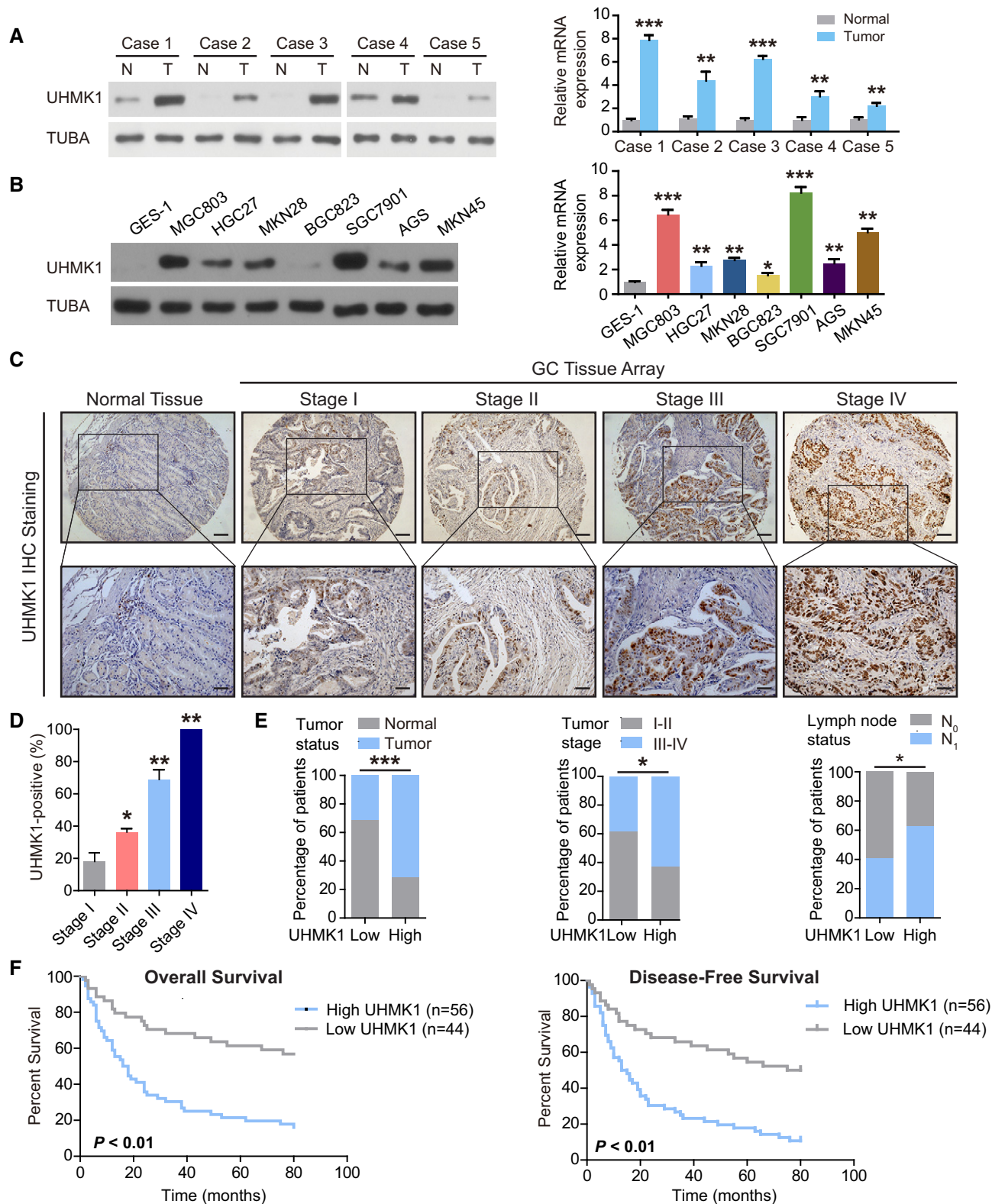


Figure 1.

(Fig 2H and Appendix Table S3). Gene ontology enrichment analysis indicated that high UHMK1 expression in GC patients might be associated mainly with tumor metabolism (Fig 2I). In summary,

UHMK1 upregulation significantly promotes GC growth and metastasis possibly via metabolic pathway reprogramming in tumors.

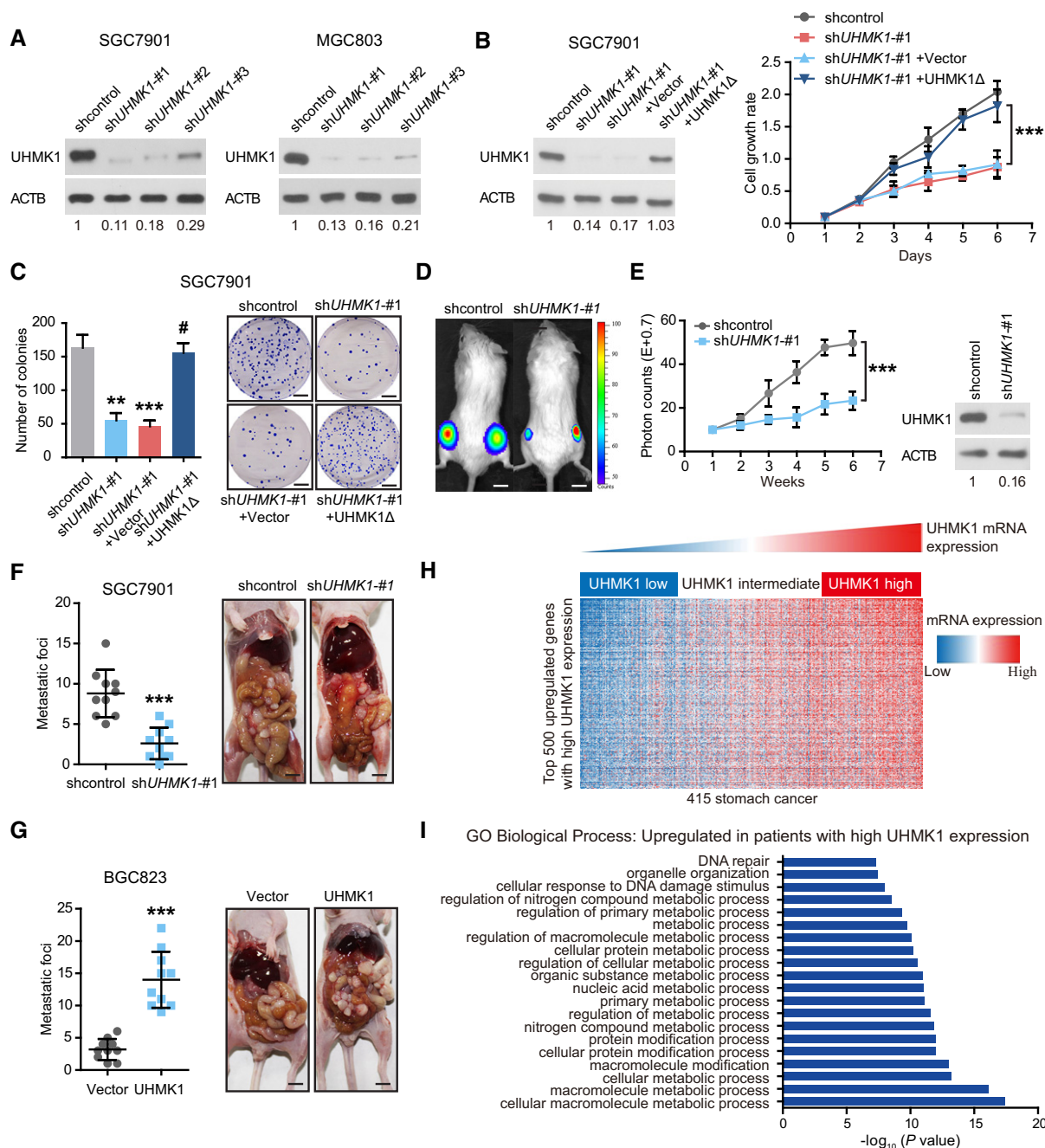


Figure 2. UHMK1 knockdown strongly suppresses the proliferative and invasive abilities of GC cells, possibly via metabolic pathway reprogramming.

A–C (A) GC cells (SGC7901 and MGC803) were transfected with (A) shUHMK1-#1, shUHMK1-#2, shUHMK1-#3, or control shRNA lentiviral vector or (B) with a shRNA-resistant expression construct, UHMK1Δ. Western blotting was used to measure the levels of UHMK1. NIH ImageJ software was used to quantify the band intensity. Western blotting assay was conducted for three replicates. (B and C) SGC7901 cells were transfected with or without shUHMK1-#1 or the shRNA-resistant expression construct UHMK1Δ. CCK-8 and colony formation assays were conducted. Scale bars = 5 mm.

D, E The volumes of subcutaneous gastric tumors derived from SGC7901 cells in NOD/SCID mice were determined at different time points. Tumors and representative bioluminescence images are also shown. UHMK1 silencing in the mouse model was confirmed by Western blotting (three biological replicates). Data were presented as mean ± standard deviation from shcontrol and shUHMK1-#1 mice (n = 10 mice/group). Unpaired two-tailed statistical significance was assessed by Student's *t*-test. Scale bars = 1 cm.

F, G UHMK1 silencing (F) and overexpression (G) affected GC cell abdominal metastasis. The quantitative number of metastatic nodules (left panel) in nude mice (n = 10 mice/group). Representative images of abdominal metastases are also shown (right panel). Scale bars = 1 cm.

H Heatmap of the top 500 genes upregulated in GC patients with high UHMK1 expression.

I Gene ontology enrichment analysis was used to analyze the top 20 enriched biological processes among GC patients with high UHMK1 expression.

Data information: ***P* < 0.01, ****P* < 0.001, # marked no significance.

UHMK1 upregulation promotes the invasion and proliferation of GC cells by promoting the *de novo* purine synthesis pathway

To examine whether UHMK1 reprograms GC-associated metabolic pathways, mass spectrometry (MS) was performed to assemble the collect metabolic profiles of SGC7901 cells with or without UHMK1 knockdown. Interestingly, UHMK1 silencing significantly reduced the intracellular pools of purine intermediates and a moderate decrease in pyrimidine metabolites (Appendix Table S4 and Fig 3A and B). Thus, silencing UHMK1 in GC cells primarily inhibits purine biosynthesis.

We then used stable isotope-labeled glutamine (amide-¹⁵N) to investigate the effect of UHMK1 on purine metabolism (Daye & Thakur, 2010). Overexpression of wild-type (WT) UHMK1 but not the kinase-dead UHMK1-K54R mutant in BGC823 cells obviously increased the amounts of ¹⁵N-purine intermediates (IMP, AMP, and GMP) (Fig 3C upper panel), suggesting that the kinase activity of UHMK1 was required for this effect of UHMK1. Additionally, silencing UHMK1 in SGC7901 cells produced the opposite effect (Fig EV3A). Second, similar findings were observed when the flux of ¹³C-glycine into purine intermediates was analyzed (Fig 3C lower panel and Fig EV3B). Third, overexpression of WT-UHMK1 but not the UHMK1-K54R mutant significantly enhanced the levels of ¹⁴C-glycine-labeled RNA and DNA in BGC823 cell line (Fig 3D), while knockdown of UHMK1 had the opposite effect (Fig EV3C). Fourth, overexpression of WT-UHMK1 but not the UHMK1-K54R mutant significantly upregulated the critical enzymes essential for activating the *de novo* purine synthesis pathway (Fig 3E). We also measured ¹⁵N-carbamoyl-L-aspartate following ¹⁵N-glutamine labeling to quantify the effects of UHMK1 on pyrimidine synthesis (Fig EV3D and E). Interestingly, we observed modest but significant decreases in pyrimidine synthesis. The changes were less dramatic than for purine synthesis. Together, these data strongly demonstrate that UHMK1 mainly activates purine synthesis in GC.

Next, we investigated the physiological significance of *de novo* purine synthesis in UHMK1-mediated GC progression. As shown in Figs 3F and EV3F and G, although UHMK1 silencing strongly inhibited the proliferative and invasive abilities of SGC7901 cells, supplementation of purine or overexpression of ATIC (a critical enzyme in the purine synthesis pathway) significantly rescued these defects in GC cells. Conversely, treatment with an ATIC inhibitor significantly

reversed the proliferation, migration, and invasion of BGC823 cells induced by UHMK1 overexpression (Figs 3G and EV3H).

Taken together, our data indicate that UHMK1 promotes GC development at least partially by reprogramming *de novo* purine metabolism.

ATF4 activation mediates UHMK1-enhanced purine biosynthesis and GC progression

Given that c-Myc, MTF, and ATF4 dictate the *de novo* purine synthesis pathway (Ben-Sahra et al, 2016; Karigane et al, 2016), we hypothesized that they might also mediate the effects of UHMK1 on GC. Interestingly, we first confirmed the expression of ATF4 and UHMK1 in BGC823 cells and further found that knockdown of ATF4 but not MTF or c-Myc significantly reversed the UHMK1-driven increase in the purine metabolic intermediates in BGC823 cells (Fig 4Ai–Aiii and Appendix Fig S1). Conversely, reintroduction of ATF4 reversed the shUHMK1-mediated effects on purine metabolism (Fig 4B). In addition, knockdown of ATF4 significantly suppressed the upregulation in the expression levels of rate-limiting genes in the *de novo* purine synthesis pathway in BGC823 cells overexpressing UHMK1 (Fig 4C). Although UHMK1 overexpression did not change the protein or mRNA levels of ATF4 (Fig 4Di and Dii), it not only enhanced ATF4 nuclear translocation but also recruited greater amounts of Pol II and ATF4 to the promoters of ATIC and PPAT (Fig 4Dii and Diii), suggesting that UHMK1 overexpression promotes purine synthesis by enhancing the transcriptional activity of ATF4.

Functionally, silencing ATF4 significantly reversed UHMK1-induced BGC823 cell proliferation, migration, and invasion (Fig 4E–G). Therefore, we concluded that ATF4 is an essential effector downstream of UHMK1 in GC.

UHMK1 interacts with and phosphorylates nuclear receptor coactivator (NCOA3) at S1062/T1067

To explore the mechanism by which UHMK1 enhances the transcriptional activation of ATF4, we used tandem mass spectrometry (MS/MS) to analyze the UHMK1 immunocomplex isolated from HEK293T cells. These proteomic data were deposited in a public database PRIDE (Appendix Table S5). We then focused on NCOA3, a critical coactivator of ATF4 (Gupta et al, 2016), which was present in the immunocomplex (Appendix Table S6). The reciprocal

Figure 3. UHMK1 upregulation significantly increases the proliferative and invasive abilities of GC cells by reprogramming purine metabolism.

- A Schematic representation of the main metabolic pathways.
- B LC-MS/MS was used to examine the metabolites in SGC7901 cells with or without UHMK1 knockdown. The data are shown in the heatmap.
- C (Upper panel) LC-MS/MS analysis was performed to measure ¹⁵N-glutamine-labeled purine synthesis intermediates in BGC823 cells transfected with or without the WT-UHMK1 or UHMK1-K54R constructs. (Lower panel) LC-MS/MS was used to analyze metabolites labeled with ¹³C-glycine in BGC823 cells transfected with or without the WT-UHMK1 or UHMK1-K54R constructs (three biological replicates).
- D RNA and DNA with incorporated ¹⁴C-glycine in BGC823 cells transfected with or without the WT-UHMK1 or UHMK1-K54R constructs were examined using LC-MS/MS (three biological replicates).
- E qRT-PCR assays were used to analyze the effects of WT-UHMK1 or UHMK1-K54R on the genes controlling purine metabolism. Data were presented as mean ± standard deviation from three replicates. Unpaired two-tailed statistical significance was assessed by Student's *t*-test.
- F UHMK1 silencing significantly decreased SGC7901 cell proliferation, while ATIC overexpression or purine supplementation markedly reversed this inhibition. Data were presented as mean ± standard deviation from three replicates. Unpaired two-tailed statistical significance was assessed by Student's *t*-test.
- G Treatment with the ATIC inhibitor significantly reversed the proliferation of BGC823 cells induced by UHMK1 overexpression. Data were presented as mean ± standard deviation from three replicates. Unpaired two-tailed statistical significance was assessed by Student's *t*-test.

Data information: **P* < 0.05, ***P* < 0.01, ****P* < 0.001, # marked no significance.

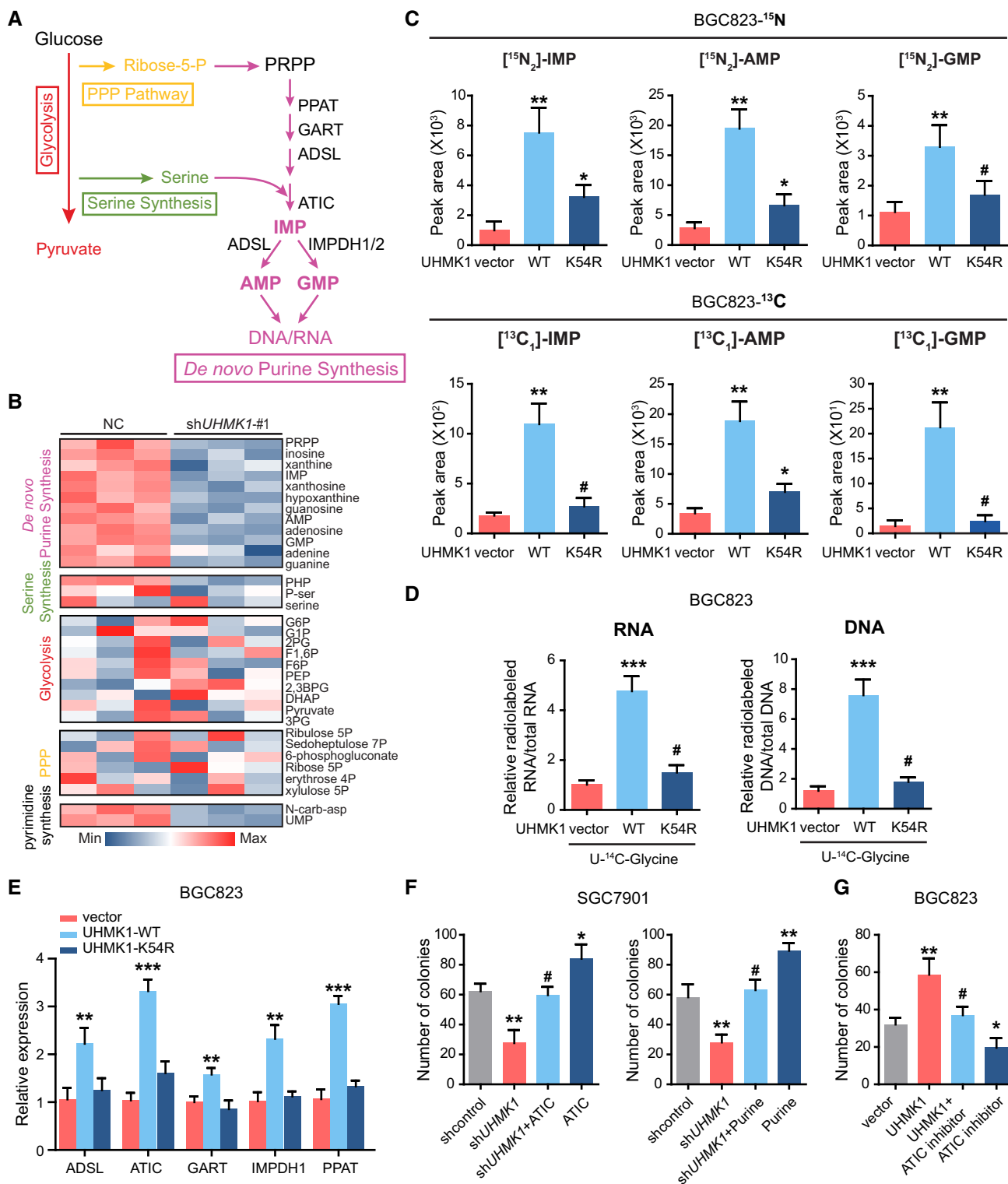


Figure 3.

immunoprecipitation in cultured BGC823 cells and pull-down assay further validated their physical interaction, respectively (Appendix Fig S2). We reasoned that NCOA3 might be a direct effector downstream of UHMK1. In support of this idea, endogenous UHMK1 was found in endogenous NCOA3 immunocomplexes in

SGC7901 cells (Fig EV4A and B). The result of co-IP assays confirmed that exogenous UHMK1 interacted with co-transfected NCOA3 in BGC823 cells (Fig EV4C). In addition, GST-UHMK1 was found to be especially effective at pulling down His-NCOA3 (Fig EV4D).

Moreover, we observed that the C-terminal domain of UHMK1, which contains a U2AF homology motif (UHM), was essential for the interaction with NCOA3 (Fig 5A). However, His-UHMK1 interacted mainly with the 922–1,161 aa fragment of NCOA3, a CBP-containing domain (CBP) (Fig 5B). These findings indicate that UHMK1 directly binds NCOA3.

To determine whether UHMK1 can phosphorylate NCOA3, different GST-NCOA3 protein fragments were used as substrates in *in vitro* kinase reactions. UHMK1 phosphorylated mainly the GST-NCOA3-CBP fragment (Fig 5C). Although the PhosphoSitePlus database predicted that 9 Ser or Thr residues within the CBP region of NCOA3 are phosphorylated, only mutation of both S1062 and T1067 to alanine (A) completely abolished the phosphorylation of the CBP domain by UHMK1 (Fig 5D). The MS/MS analysis results further confirmed that UHMK1 phosphorylated NCOA3 at S1062/T1067 in BGC823 cells overexpressing UHMK1 (Fig EV4E).

To easily show the importance of UHMK1 in mediating NCOA3 phosphorylation at S1062/T1067 *in vivo*, we produced a phospho-specific antibody (Ab) against the S1062/T1067 residues. Two experiments were performed to validate this new phospho-S1062/T1067 NCOA3 antibody (Appendix Fig S3). Using this antibody, we found that knockdown of endogenous *UHMK1* in SGC7901 cells significantly suppressed NCOA3 phosphorylation at S1062/T1067 (Fig 5E), and this antibody did not recognize the S1062E/T1067E and S1062A/T1062A mutants (Appendix Fig S3). Collectively, our data indicate that UHMK1 directly phosphorylates NCOA3 at S1062/T1067.

UHMK1-dependent phosphorylation of NCOA3 at S1062/T1067 promotes GC progression by activating purine synthesis

We then examined the physiological significance of NCOA3 phosphorylation by UHMK1 at S1062/T1067. The data in Fig 6A indicate that *UHMK1* knockdown in SGC7901 cells strongly impaired the interaction of NCOA3 with ATF4. However, overexpression of UHMK1 in BGC823 cells promoted the binding of ATF4 to WT-NCOA3 but not to the NCOA3-S1062A/T1067A mutant (Fig 6B).

These findings were further confirmed via a proximity ligation assay (PLA) (Fig 6C). Computational modeling of the structures predicted by ZDOCK software showed that phosphorylation of both S1062 and T1067 was essential for the direct binding of NCOA3 to ATF4 (Fig 6D; Li *et al*, 2007).

Consistent with these findings, exogenous expression of the NCOA3-S1062E/T1067E but not the NCOA3-S1062A/T1067A mutant significantly promoted the binding of the NCOA3/ATF4 complex to the promoters of critical metabolic genes in the purine pathway (Fig 6Ei), consequently enhancing their expression (Fig 6Eii).

Interestingly, both WT-NCOA3 and NCOA3-S1062E/T1067E, phosphomimetic construct, significantly enhanced GC aggressiveness in nude mice, while the NCOA3-S1062A/T1067A construct exhibited the opposite effect (Fig 6F–H).

Therefore, we propose that NCOA3-S1062/T1067 phosphorylation promotes GC progression by activating purine synthesis.

ATF4 enhances UHMK1 transcription in GC cells

To determine whether ATF4 acts upstream of UHMK1 in GC, we treated SGC7901 and MGC803 cells with *ATF4* siRNA. Interestingly, knockdown of *ATF4* significantly decreased the protein and mRNA levels of UHMK1 (Fig 7A). However, overexpression of ATF4 had the opposite effects in BGC823 and HGC27 cells (Fig 7B).

Sequence analysis of the *UHMK1* promoter indicated two putative ATF4 binding motifs (Fig 7C). After mutation of these two sites, the activity of *UHMK1*-luciferase reporters was significantly decreased (Fig 7D). Thus, ATF4 transcriptionally activates the *UHMK1* promoter via these motifs.

The results of chromatin immunoprecipitation (ChIP) assays further showed ATF4 recruitment to the *UHMK1* promoter in GC cell lines (Fig 7E). Consistent with this finding, increasing ATF4 expression in BGC823 and HGC27 cells enhanced *UHMK1* promoter activity, while *ATF4* knockdown in SGC7901 and MGC803 cells had the opposite effect (Fig 7F). Therefore, ATF4 promotes *UHMK1* transcription in GC, thus forming a positive feedback loop.

Figure 4. ATF4 activation mediates UHMK1-enhanced purine biosynthesis and GC progression.

- A (Ai) Western blot analysis was used to confirm UHMK1 overexpression and *ATF4* knockdown in BGC823 cells. (Aii) Silencing *ATF4* significantly decreased the levels of the indicated metabolites in BGC823 cells overexpressing UHMK1 (three biological replicates). (Aiii) Silencing *ATF4* significantly decreased the levels of RNA and DNA containing U-¹⁴C-glycine in BGC823 cells overexpressing UHMK1 (three biological replicates)
- B LC-MS/MS was used to examine the metabolites in SGC7901 cells with or without *UHMK1* knockdown or *ATF4* reintroduction. The data are shown in the heatmap.
- C Silencing *ATF4* significantly decreased the levels of the indicated genes in BGC823 cells overexpressing UHMK1. Data were presented as mean \pm standard deviation from three replicates. Unpaired two-tailed statistical significance was assessed by Student's *t*-test.
- D (Di) qRT-PCR was used to measure the expression of ATF4 in BGC823 cells overexpressing UHMK1. (Dii) UHMK1 overexpression enhanced the nuclear translocation of ATF4 in BGC823 cells. (Diii) ChIP assays on the ATIC and PPAT promoters were performed in BGC823 cells with the indicated antibody. Data were presented as mean \pm standard deviation from three replicates. Unpaired two-tailed statistical significance was assessed by Student's *t*-test.
- E Silencing *ATF4* markedly decreased the proliferation of BGC823 cells overexpressing UHMK1. (Left panel) The quantitative number of colonies formed in scramble+Flag, scramble+Flag-UHMK1, siATF4+Flag, and siATF4+Flag-UHMK1 group. Data were presented as mean \pm standard deviation from three replicates. Unpaired two-tailed statistical significance was assessed by Student's *t*-test. (Right panel) Representative images of colonies are shown. Scale bars = 5 mm.
- F Silencing *ATF4* markedly decreased the migration of BGC823 cells with UHMK1 overexpression. (Left panel) The quantitative number of migrated cells in scramble+Flag, scramble+Flag-UHMK1, siATF4+Flag, and siATF4+Flag-UHMK1 group. Data were presented as mean \pm standard deviation from three replicates. Unpaired two-tailed statistical significance was assessed by Student's *t*-test. (Right panel) Representative images of migrated cells in each group are shown. Scale bars = 100 μ m.
- G Silencing *ATF4* markedly decreased the invasion of UHMK1 overexpressing BGC823 cells. (Left panel) The quantitative number of invaded cells in scramble+Flag, scramble+Flag-UHMK1, siATF4+Flag, and siATF4+Flag-UHMK1 group. Data were presented as mean \pm standard deviation from three replicates. Unpaired two-tailed statistical significance was assessed by Student's *t*-test. (Right panel) Representative images of invaded cells in each group are shown. Scale bars = 100 μ m.
- Data information: **P* < 0.05, ***P* < 0.01, ****P* < 0.001, # marked no significance.

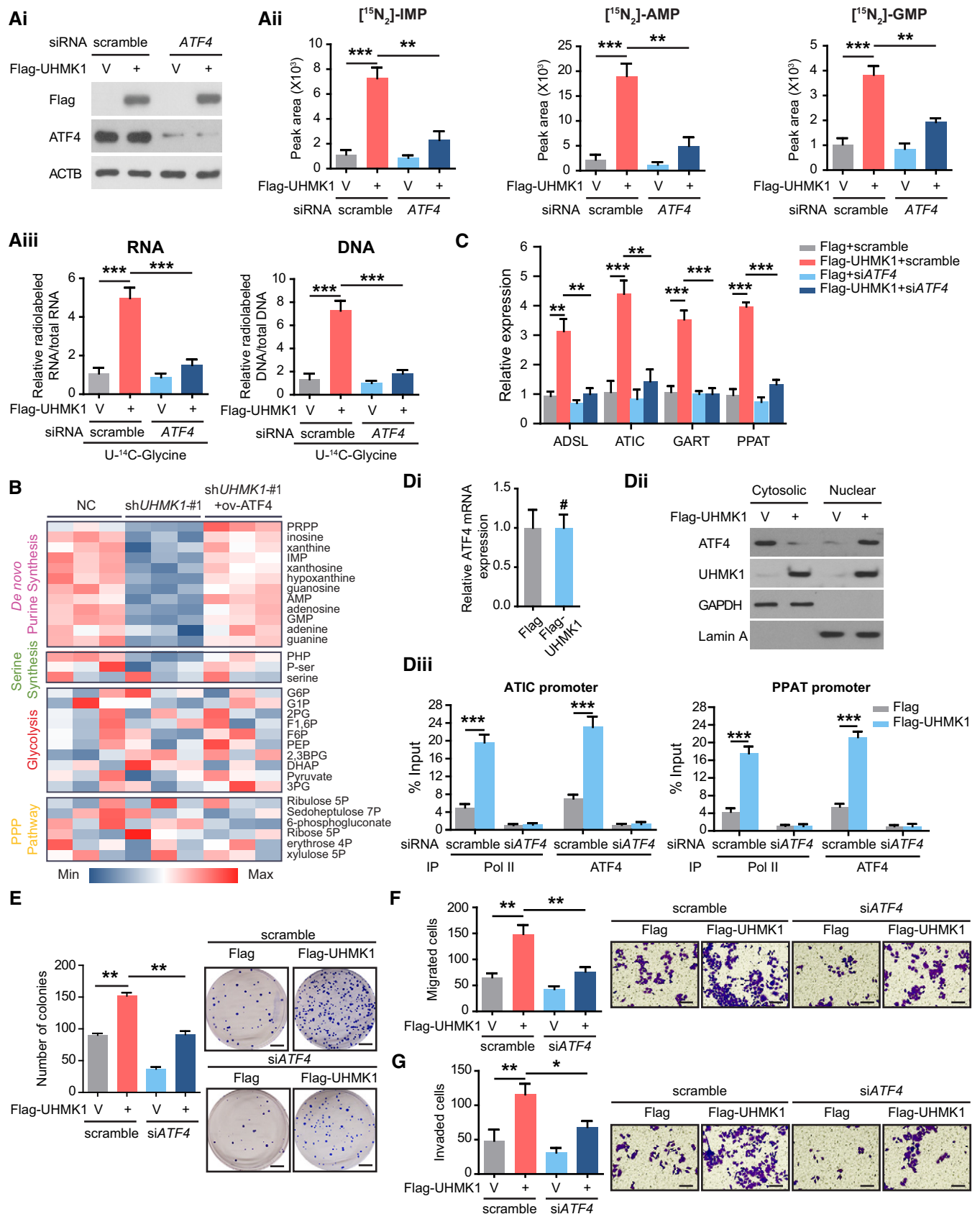


Figure 4.

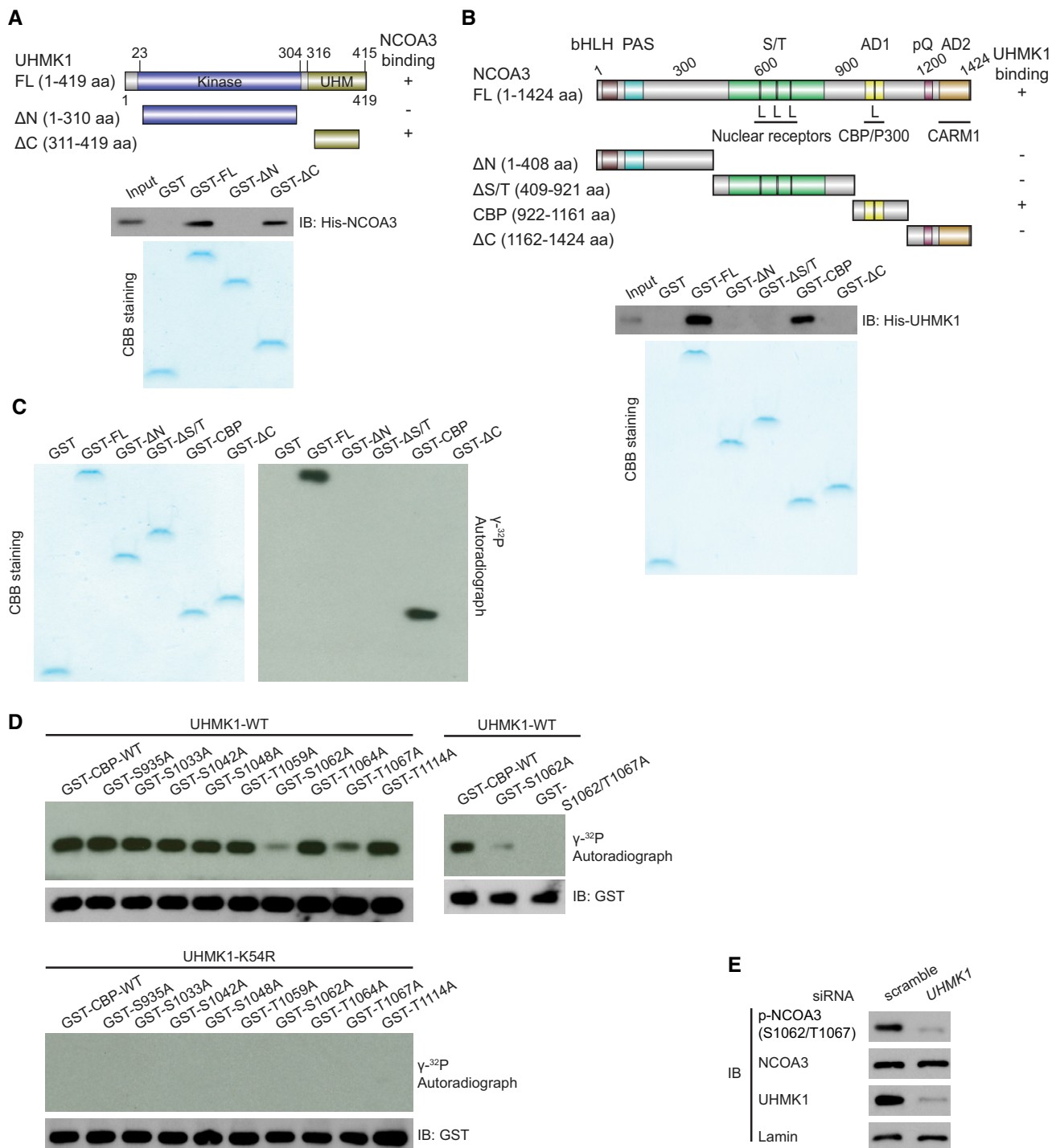


Figure 5. UHMK1 interacts with and phosphorylates NCOA3 at S1062/T1067.

- A GST-UHMK1 full length (FL), GST-UHMK1 ΔN (N-terminal truncated, 1–310aa), and GST-UHMK1 ΔC (C-terminal truncated, 311–419aa) were constructed (upper panel). GST-labeled FL, ΔN, and ΔC protein fragments were incubated with His-NCOA3. Pull-down, Coomassie blue staining, and Western blotting were performed (lower panel).
- B GST-NCOA3 full length (FL), GST-NCOA3 ΔN (1–408aa), GST-NCOA3 ΔS/T (409–921aa), GST-NCOA3 CBP (922–1,161aa), and GST-NCOA3 ΔC (1,162–1,424aa) were constructed (upper panel). Pull-down assay with GST-NCOA3 FL or its protein fragments (ΔN, ΔS/T, CBP, and ΔC) and His-UHMK1 were performed (lower panel).
- C We performed an *in vitro* kinase assay by incubating purified NCOA3 FL or its protein fragments with purified UHMK1 kinase. These proteins were visualized using Coomassie blue staining. The phosphorylation of the substrates is shown in the autoradiograph.
- D WT-UHMK1 or kinase-dead UHMK1-K54R protein was mixed with GST-CBP-WT or the indicated mutant, and *in vitro* kinase assays were performed.
- E Silencing *UHMK1* in SGC7901 cells via *UHMK1*-siRNA. NCOA3 phosphorylation at S1062/T1067 was measured with a special Ab that recognizes phosphorylated NCOA3-S1062/T1067.

***Helicobacter pylori* infection and GC-associated UHMK1 mutation significantly enhance UHMK1 activity and NCOA3 phosphorylation at S1062/T1067 in GC**

Since ATF4 activation was found to be significantly associated with *H. pylori*-positive GC (Diaz et al, 2018), we examined

whether *H. pylori* infection affected UHMK1 expression, NCOA3 phosphorylation at S1062/T1067, and ATF4 transcriptional activity in GC.

Interestingly, in BGC823 cells treated with or without J166 or 7.13 (two *Cag*⁺ *H. pylori* strains) (Souitto et al, 2015), the expression of UHMK1 mRNA and protein was significantly upregulated

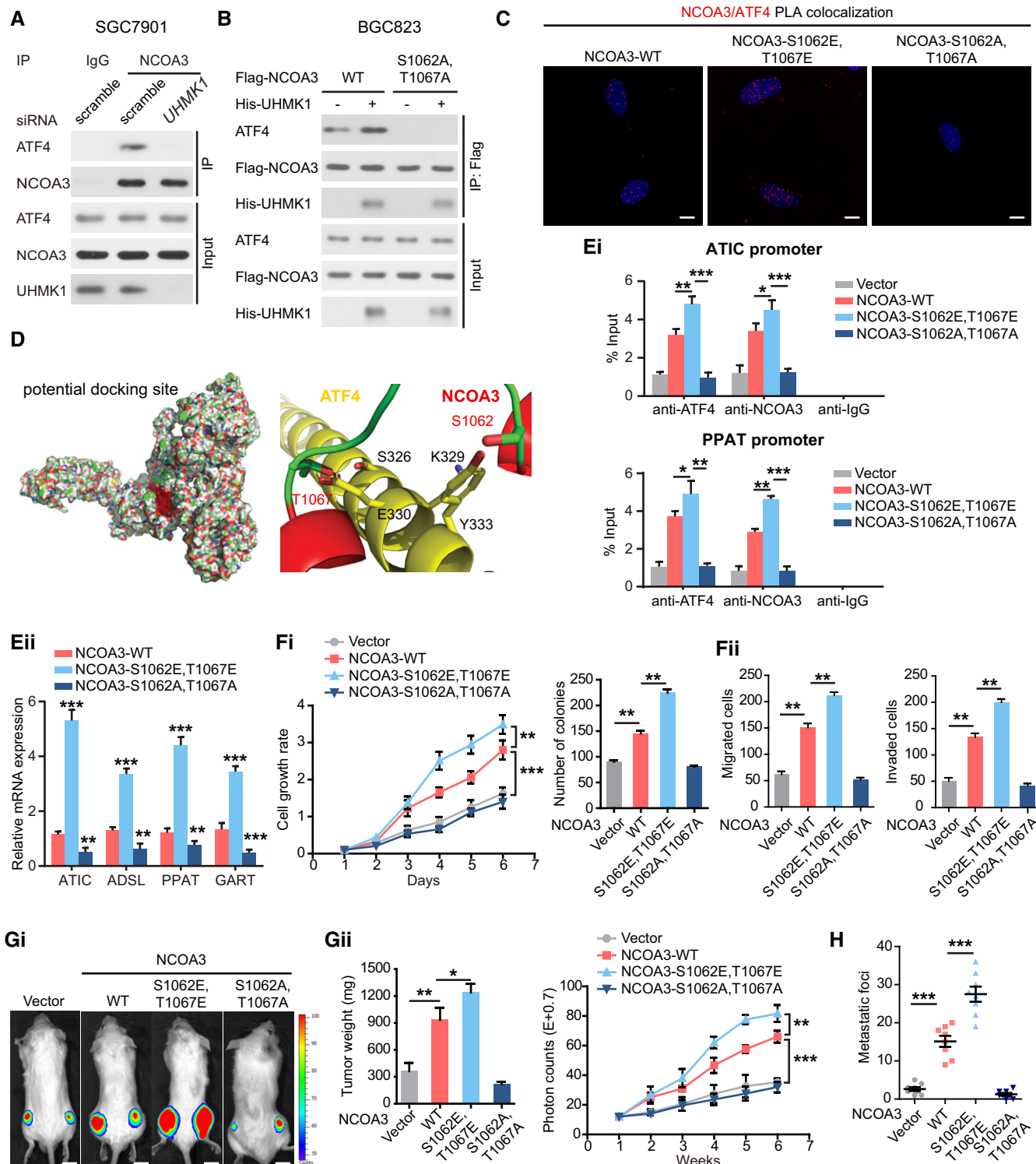


Figure 6.

Figure 6. UHMK1-dependent phosphorylation of NCOA3 at S1062/T1067 promotes GC progression by promoting the *de novo* purine synthesis pathway.

- A Knockdown of *UHMK1* blocked NCOA3 binding to ATF4. SGC7901 cells were treated as indicated. Co-IP was carried out with mouse immunoglobulin G (IgG) or anti-NCOA3 antibody. Then, Western blotting was performed.
- B BGC823 cells were transfected with Flag-NCOA3 or NCOA3-S1062A/T1067A with or without His-tagged UHMK1. Co-IP was performed using an anti-Flag antibody.
- C Proximity ligation assay of the interaction between different NCOA3 proteins and ATF4 in BGC823 cells. Confocal images were acquired with a Nikon A1 microscope and the Nikon Elements software suite. Maximum projection images are shown (original magnification $\times 120$). Scale bars = 20 μm .
- D Computational molecular docking analysis to investigate the molecular mechanism by which NCOA3-S1062/T1067 phosphorylation is involved in the interaction of NCOA3 binding to ATF4. Based on the predictions of ZDOCK software, S1062 and T1067 of NCOA3 are located in the interface between ATF4 and NCOA3, and S1062/T1067 phosphorylation greatly enhances the binding affinity of NCOA3 for ATF4 by increasing NCOA3 hydrophilicity.
- E (Ei) ChIP data from BGC823 cells are presented as indicated. (Eii) NCOA3-S1062/T1067 phosphorylation by UHMK1 enhanced the expression of critical genes as indicated (three biological replicates).
- F (Fi and Fii) The effects of WT-NCOA3 and the NCOA3-S1062A/T1067A, and NCOA3-S1062E/T1067E mutants on BGC823 cell proliferation, invasion, and migration (three biological replicates).
- G, H The effects of WT-NCOA3, and the NCOA3-S1062A/T1067A, and NCOA3-S1062E/T1067E mutants on GC growth and metastasis in the mouse model ($n = 10$ mice/group). Scale bars = 1 cm.

Data information: Unpaired two-tailed statistical significance was assessed by Student's *t*-test. Data represent mean \pm SD. * $P < 0.05$, ** $P < 0.01$, *** $P < 0.001$.

(Fig 8A and B). When the *Cag*⁺ *H. pylori* strain PMSS1 or Brucella broth (as the negative control) was used to challenge mice (Noto *et al*, 2019), PMSS1 infection significantly enhanced the levels of *UHMK1* mRNA and protein compared to those in control mice (Fig 8C and D). Moreover, *H. pylori* infection significantly enhanced NCOA3 phosphorylation at S1062/T1067 but did not markedly affect the total levels of NCOA3 and ATF4 (Fig 8B and D).

We also evaluated whether *H. pylori* challenge affected the transcriptional activity of ATF4. As shown in Fig 8E, significant induction of ATF4 transcriptional activity was observed in BGC823 cells infected with *H. pylori* strain J166 or 7.13.

Although TCGA data analysis identified three somatic missense mutations of *UHMK1* in human GC (Fig 8Fi), the functions of these mutations were not elucidated. As shown in Fig 8Fii, the M134T and T217K mutations, which are located in the kinase domain, greatly increased the activity of *UHMK1*, while the A18V mutation produced no obvious effect. The M134T and T217K mutations also upregulated NCOA3 phosphorylation at S1062/T1067 (Fig 8Fiii). Importantly, the M134T and T217K mutations strongly promoted GC cell proliferation and invasion (Fig 8G and H).

Taken together, these results indicate that *H. pylori* infection and GC-associated *UHMK1* mutations significantly enhance *UHMK1* activity, NCOA3 phosphorylation at S1062/T1067, and ATF4 activity in GC cells both *in vitro* and *in vivo*.

Clinical correlations of UHMK1 with p-NCOA3 (S1062/T1067) and ATIC in GC patients' tissues

To further reveal the clinical significance of our data, we examined the correlations of *UHMK1* with p-NCOA3 (S1062/T1067) and ATIC in 120 GC patient samples. The results of immunohistochemistry (IHC) assays indicated significant positive correlations between these markers (Figs 9A and EV5, Appendix Tables S7 and S8). These findings were further validated using Pearson's correlation analysis (Fig 9Bi and Bii). The Kaplan–Meier data indicated that a high level of *UHMK1* or p-NCOA3 (S1062/T1067) in GC was markedly associated with poor OS (Fig 9C). Collectively, these findings suggest that targeting the *UHMK1*/NCOA3/ATF4 axis might be critical in the treatment of GC (Fig 9D).

Discussion

This report, for the first time, elucidated an important role of the *UHMK1* kinase in the reprogramming of GC metabolism. We demonstrated that (i) *UHMK1* is significantly upregulated in GC tissues compared to normal control tissues, and silencing *UHMK1* in GC cells strongly inhibits tumor aggressiveness; (ii) the roles of *UHMK1* in GC are mediated at least partially via activation of the *de novo* purine synthesis pathway; (iii) this action of *UHMK1* requires ATF4 and its key coactivator NCOA3; (iv) *UHMK1* directly phosphorylates NCOA3 at S1062 and T1067, thereby increasing its binding to ATF4 and the expression of purine metabolism-associated target genes; (v) *H. pylori* infection and human GC-associated *UHMK1* mutations (M134T and T217K) induce NCOA3-S1062/T1067 phosphorylation and enhance *UHMK1* activity; and (vi) the level of *UHMK1* is significantly correlated with the level of phospho-NCOA3 (S1062/T1067) and ATIC in human GC specimens. Together, our data elucidate a previously unrecognized mechanism that is operational in GC, thus paving a path to identify novel GC therapies.

In contrast to the extensive knowledge about the PI3K/AKT and MAPK kinase signaling pathways (Matsuoka & Yashiro, 2014), very little is known about *UHMK1*, its upstream activators, and its downstream targets, let alone its action mechanisms in carcinogenesis. Although all three known substrates of *UHMK1* (p27^{KIP1}, FAM64A, and SF1) have been shown to be involved in carcinogenesis and *UHMK1* positively modulates cell cycle progression in untransformed cells (Boehm *et al*, 2002; Manceau *et al*, 2008; Cambray *et al*, 2009), the functions of *UHMK1* in GC development are unclear. Here, we demonstrated that *UHMK1* upregulation in advanced GC significantly promotes its growth and dissemination, strongly indicating that *UHMK1* functions as an oncogene and should be considered as a candidate therapeutic target in this deadly and invasive disease.

Metabolite analysis has recently become an active area of investigation because it may facilitate the understanding of metabolic dysregulation in cancer and the function of cancer-related genes in disease processes (Sullivan *et al*, 2016). One consideration in this study is that MS/MS-based profiling of metabolites might be a very good tool to uncover the molecular mechanisms of *UHMK1* in GC progression. Indeed, via this method, this study revealed a new function of *UHMK1* in promoting purine metabolism, not glycolysis

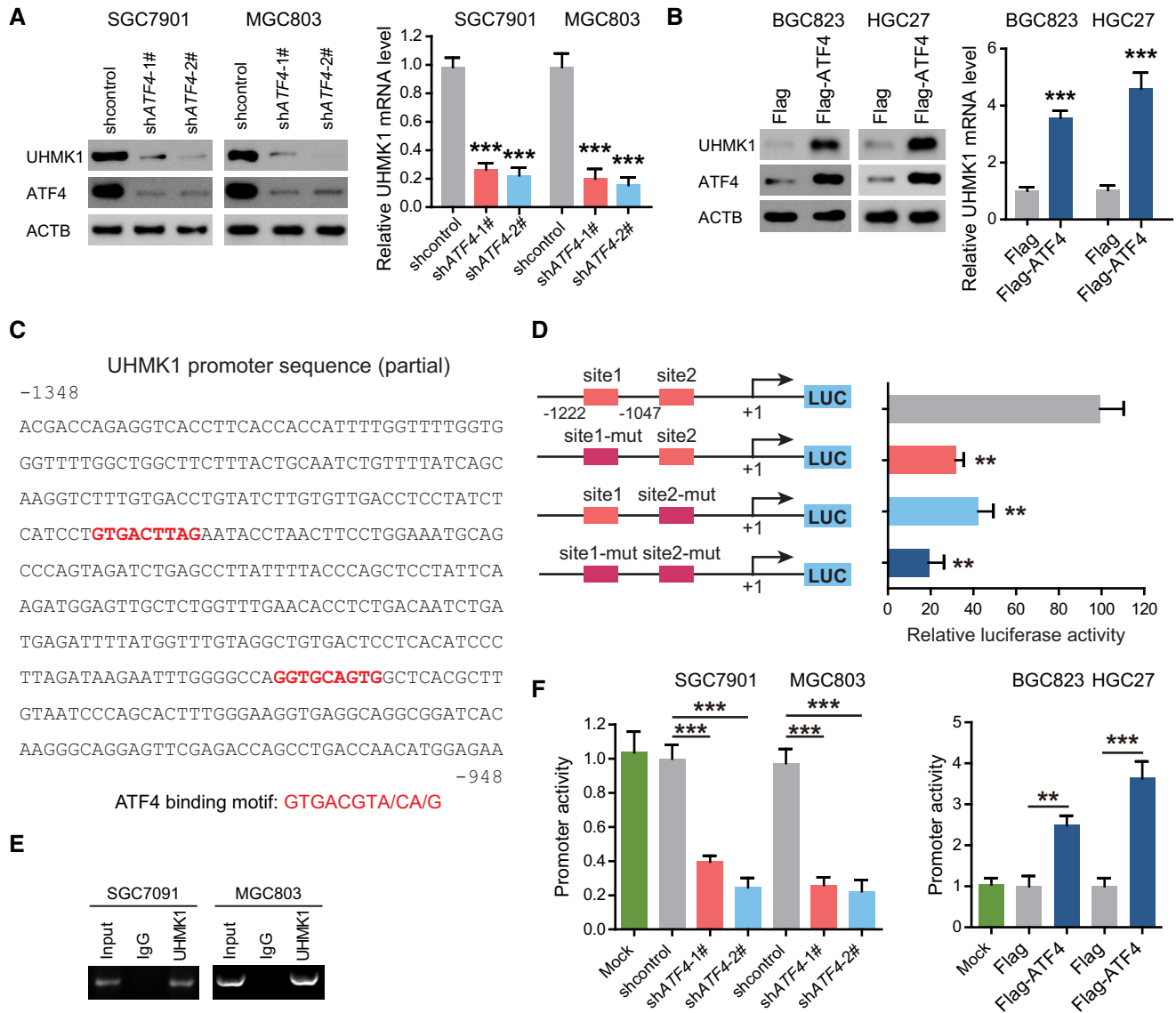


Figure 7. ATF4 directly activates the transcription of the UHMK1 promoter in GC.

A SGC7901 and MGC803 cells were transfected with ATF4 shRNA or shcontrol. Western blottings and qRT-PCR were used to analyze the expression of UHMK1. Data were presented as mean \pm standard deviation from three replicates. Unpaired two-tailed statistical significance was assessed by Student's *t*-test.

B Overexpression of ATF4 enhanced the expression of UHMK1 in BGC823 and HGC27 cells. Data were presented as mean \pm standard deviation from three replicates. Unpaired two-tailed statistical significance was assessed by Student's *t*-test.

C The nucleotide sequences showing the -1,348/-948 region in the human *UHMK1* gene. The red text indicates the candidate ATF4 binding sites.

D The effect of ATF4 on the activity of the WT-*UHMK1* promoter and its mutations, as evaluated by using luciferase reporter assays.

E ChIP assays were used to examine the binding of ATF4 to the *UHMK1* promoter in SGC7901 and MGC803 cells. Input DNA and nonspecific IgG were included as controls.

F ATF4 deficiency and overexpression regulated the activity of the *UHMK1* promoter in GC cells.

Data information: Data represent mean \pm SD. ***P* < 0.01, ****P* < 0.001.

and the PPP pathway, in GC cells. Our data and other reports indicate that metabolomics is a powerful technology currently used not only to discover diagnostic cancer biomarkers in the clinic, but also to clarify functional pathways involved in cancer (Burton & Ma, 2019). In accordance with the above idea, NCOA3 was identified as a novel substrate of UHMK1, and ATF4 but not c-Myc or MITF was identified as its downstream effector in GC. Therefore, our findings

uncover a previously unrecognized molecular mechanism of UHMK1 in GC development. Although our results indicate the critical role of this UHMK1-NCOA3-ATF4 axis in GC, the ATF4 knockdown has effects independent of UHMK1. For example, ATF4 knockdown inhibits glycolysis and serine metabolism besides purine synthesis (Yoshizawa *et al*, 2009; Selvarajah *et al*, 2019). On the other hand, the previous studies indicate that not all of ATF4 effects

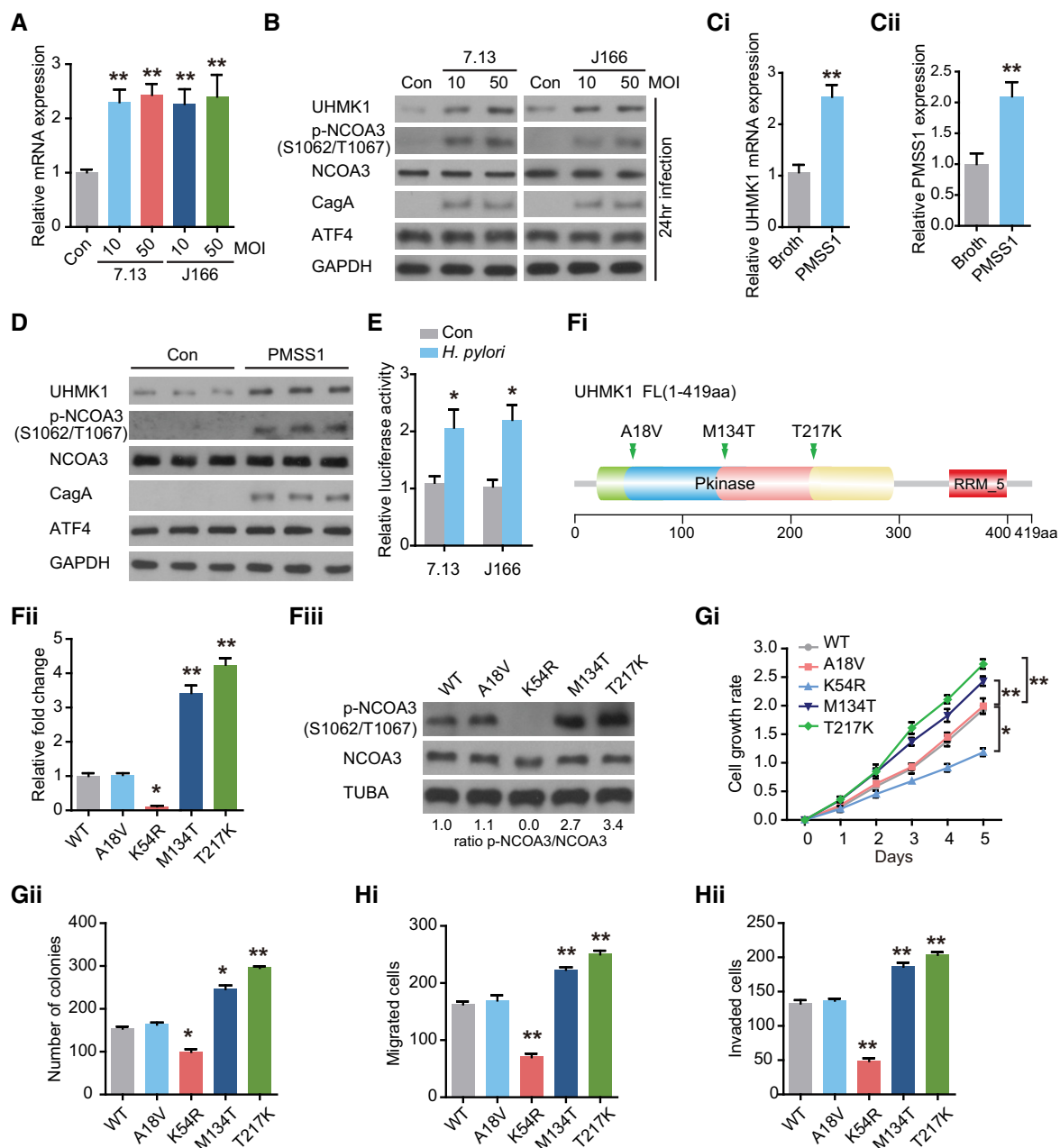


Figure 8. *H. pylori* infection and GC-associated UHMK1 mutation significantly enhance UHMK1 activity, NCOA3 phosphorylation at S1062/T1067, and ATF4 activity in GC.

A qRT-PCR was performed to analyze UHMK1 expression in BGC823 cells infected with or without *H. pylori* CagA⁺ strains 7.13 and J166. MOI, multiplicity of infection. Data were presented as mean \pm standard deviation from three replicates.

B Immunoblotting of UHMK1, NCOA3 phosphorylated at S1062/T1067, NCOA3, and ATF4 in the samples from (A).

C PMSS1, a *H. pylori* strain, was used to challenge mice orogastrically, with Brucella broth as the control. qRT-PCR was performed to measure UHMK1 (Ci) and PMSS1 (Cii) expression in gastric tissues. Data were presented as mean \pm standard deviation from three replicates.

D Immunoblotting of UHMK1, NCOA3 phosphorylated at S1062/T1067, NCOA3, and ATF4 in the samples from (C).

E An ATF4 luciferase reporter assay was carried out in BGC823 cells with or without *H. pylori* infection. Data were presented as mean \pm standard deviation from three replicates.

F (Fi) The domain architecture of UHMK1 and the positions of human GC-associated mutations. (Fii and Fiii) IP kinase assay. Briefly, UHMK1 from HEK293 cells expressing WT-UHMK1 or its mutants was immunoprecipitated with anti-HA antibodies. The immunoprecipitated proteins were mixed with a synthetic peptide of the CATS protein (a known substrate of UHMK1) and [³²P] ATP. A phosphocellulose paper assay was used to measure kinase activity. The results were normalized to a value of 1.0 for WT-UHMK1 (three biological replicates).

G The effects of human GC-associated UHMK1 mutations on the proliferation and colony formation of GC cells (three biological replicates).

H The effects of human GC-associated UHMK1 mutations on GC cell invasion and migration (three biological replicates).

Data information: Unpaired two-tailed statistical significance was assessed by Student's *t*-test. Data represent mean \pm SD. **P* < 0.05, ***P* < 0.01.

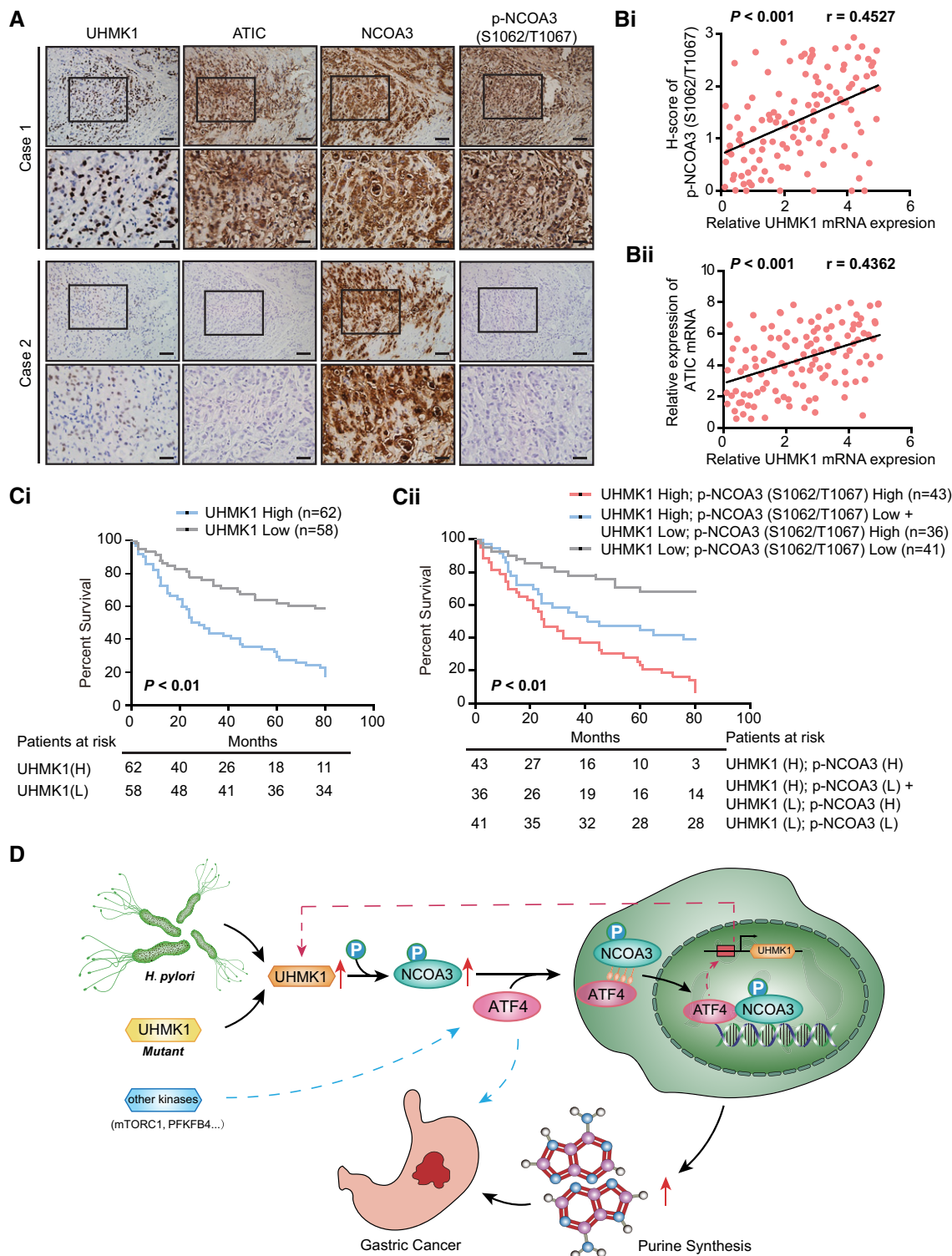


Figure 9. Clinical correlations of UHMK1 with p-NCOA3 (S1062/T1067) and ATIC in human GC samples.

A Images showing UHMK1, p-NCOA3 (S1062/T1067), and ATIC protein expression in two human GC specimens. Scale bars = 100 μ m.
 B Pearson's correlation analysis about of the levels of UHMK1, p-NCOA3 (S1062/T1067), and ATIC proteins in patients with GC ($n = 120$) by IHC.
 C (Ci) OS data from GC patients stratified by the level of UHMK1. (Cii) Combination of UHMK1 and p-NCOA3 (S1062/T1067) expression predicts more exact OS of GC patients. Survival curves were plotted according to Kaplan–Meier method, with the log-rank test applied for comparison.
 D Schematic depicting the function of UHMK1 in GC. *H. pylori*-induced upregulation of UHMK1 or human GC-associated UHMK1 mutation enhances the level of NCOA3 phosphorylation at S1062/T1067; this event greatly increases the association of NCOA3 with ATF4, which activates the *de novo* purine biosynthesis pathway and promotes the development of GC. Interestingly, activated ATF4 transcriptionally upregulated UHMK1 expression.

are due to UHMK1's modulation of ATF4. Other kinases such as mTORC1 and 6-phosphofructo-2-kinase/fructose-2,6-biphosphatase 4 (PFKFB4) have been shown to activate ATF4 (Ben-Sahra *et al*, 2016; Dasgupta *et al*, 2018).

Notably, there have been a number of recent advances in approaches utilizing small-molecule inhibitors of purine metabolism-related kinases for treating cancer. For example, the selective cytotoxicity of inhibitors of GART and IMPDH, two core enzymes in *de novo* purine synthesis, has been clinically tested in acute lymphoblastic leukemia (ALL) (Li *et al*, 2015). Additional enzymes in the purine metabolic pathway might be suitable targets for the treatment of chemoresistant ALL (Bouzar *et al*, 2009). Our studies in GC further support this idea. In this context, these inhibitors could also impact the prevention or treatment of GC. Therefore, targeting of the purinosome might be an important future research direction.

The results outlined in this paper parallel those in a previous report, indicating that the NCOA3/ATF4 complex plays a critical role in the purine metabolism in breast cancer (Dasgupta *et al*, 2018). In that report, the authors propose that PFKFB4 phosphorylates NCOA3 at S857, resulting in upregulation of ATF4 transcriptional activity (Dasgupta *et al*, 2018). However, we clearly demonstrated that in GC, an alternate kinase, UHMK1, is involved in the functional enhancement of NCOA3. Our observations are not unexpected, because several domains of NCOA3 can bind to various proteins and multiple Ser/Thr sites in NCOA3 have been predicted to be phosphorylated by different kinases. Here, we identified UHMK1 as a new kinase of NCOA3 via phosphorylation of S1062/T1067. Although further study is required to clarify the differences in the applicability of these mechanisms in various tumors, targeting S1062/T1067 phosphorylation may be an effective therapeutic approach for GC with UHMK1 overexpression. This conclusion is further supported by the following data: (i) *H. pylori* infection induced NCOA3-S1062/T1067 phosphorylation and enhanced the promoter activity of UHMK1 via ATF4; and (ii) GC-associated UHMK1 mutation promoted its binding to NCOA3 and its activity. Of course, we did not rule out the possibility that PFKFB4 might also contribute to GC. But this was beyond the scope of this work.

By analyzing the public Oncomine database, we found that the DNA level of UHMK1 is also frequently increased in liver cancer (Appendix Fig S4). Based on our findings in GC, it is tempting to speculate that the UHMK1-enhanced purine synthesis pathway might similarly be involved in hepatoma carcinogenesis. If so, these results support the idea that UHMK1 does not selectively promote GC but may universally affect cancers of the digestive system. Future studies should explore the potential therapeutic benefit of targeting UHMK1 in diverse tumor types.

In summary, this study provides strong evidence that UHMK1 contributes to purine metabolism reprogramming in GC by regulating the NCOA3/ATF4 axis, suggesting that UHMK1 might be a potential biomarker and attractive therapeutic target for GC.

Materials and Methods

Cell culture, reagents, and antibodies

HEK293T, gastric epithelium cells (GES-1 as control), and gastric cancer (GC) cells (MKN28, BGC823, HGC27, MGC803, MKN45, and

SGC7901) were provided by American Type Culture Collection and passed as described (Yusefi *et al*, 2018; Zhu *et al*, 2019). 13C-glycine, 15N-glutamine, fetal bovine serum (FBS), and protease inhibitor cocktail were obtained from Santa Cruz. 14C-Glycine was from PerkinElmer. Lipofectamine 2000, PBS, antibiotics, and DMEM were purchased from Invitrogen. Tween-20 and X-film were provided by Sigma. Site-Directed Mutagenesis Kit (Agilent) was from QuikChange II. Anti-Flag M2-conjugated agarose was from Sigma. Anti-UHMK1 (Santa Cruz Biotechnology, sc-393605), PRPS2 (Abcam #ab55918), NCOA3 (Santa Cruz Biotechnology, #sc25742), ADSL (GeneTex #GTX84956), ATF4 (Santa Cruz Biotechnology #sc390063), GAPDH (Abcam #ab9485), IMPDH1 (Abcam #ab33039), Actin (Abcam #ab8226), PPAT (Abcam #ab204366), c-Myc (Abcam #ab39688), ATIC (Zymed Laboratories Inc., #410100), MITF (Abcam #ab20663), GART (Proteintech #13659-1-AP), Lamin A (Abcam #ab26300), PPAT (Proteintech #15401-1-AP), secondary antibodies (Bio-Rad, #1706515 and #1706516), and pS1062/T1067-NCOA3-specific antibody were made by this laboratory using the similar methods as described previously (Hong *et al*, 2018).

ShRNA, siRNA, and plasmids

For shRNA transfection, 6-well plates were used to culture MGC803 and SGC7901 cells overnight prior to transfection (about 2×10^5 cells/well). As previously reported (Hong *et al*, 2014), they were transduced through spinoculation with three different shRNAs against UHMK1 (shUHMK1-#1, shUHMK1-#2, and shUHMK1-#3) or shcontrol with lentivirus particles at multiplicity of infection (MOI) about 1. After about two weeks of antibiotic selection (1 μ g/ml) later, stable polyclonal GC cell lines with shcontrol or shUHMK1 were established. For siRNA transfection, Lipofectamine 2000 (Invitrogen) was used to perform siRNA transfection for siATF4, siMyc, siMITF, or scramble negative control (Invitrogen) following the protocol. Immunoblots were used to determine the efficiency of knockdown at 2 days after transfection. All siRNAs and shRNA were as follows: shUHMK1-#1: 5'-CCAGAAGCAGAAUUGCAAATT-3'; shUHMK1-#2: 5'-GAUGCUUGAUCUUGCACAATT-3'; shUHMK1-#3: 5'-UCUUCUUUAUUGUUGATT-3'; or shcontrol: 5'-AATGCTCGCACAGCACAAG-3' (Santa Cruz Biotechnologies); and siPPAT: 5'-GAA AUGGUCUGGAAUGUUU-3'; siMITF: 5'-GAAACUUGAUCGAC CUCU ACA-3' and 5'-UAGAGGUCGAUCAAGUUUCCA-3'; siATIC: 5'-CAGUCUAACUCUGUGUCUACGCCA-3'; siATF4: 5'-CCACGUAUG ACACUUGdTdT-3'; siMyc: 5'-TCC GTA CAG CCCTATTTC-3' (Invitrogen); a shRNA-resistant mutant UHMK1 Δ was constructed by making five silent mutations at CDS area (534G > C, 537 T > A, 541 A > T, 551 T > C, and 554 C > A) against UHMK1 shRNA.

Human UHMK1 construct (OriGene, RC214962) was purchased from OriGene. Human ATF4 plasmid was purchased from Addgene Plasmid (Cat: #26114). NCOA3 vector was from Dr. Bingbing Wang at the State University of New Jersey. Mutants or truncated fragments from different genes such as UHMK1 and NCOA3 were constructed as described previously (Song *et al*, 2018). And sequencing was used to verify the resulting mutants.

The sample collection of GC patients

In this study, tissue samples of all GC patients and corresponding nontumor gastric samples were collected at the Affiliated Hospital,

Harbin Medical University, from 2012 to 2017. This study ethical was passed by the Harbin Medical University Institute Research Ethics Committee. And all informed consents were taken from each GC participant. All tumor tissues for RNA isolation and immunohistochemistry (IHC) were histopathologically confirmed by a pathologist. Tumor–node–metastasis (TNM), a cancer staging system, was used to define the histological type and cancer stage according to the American Joint Committee (the 7th edition).

Western blot

GC tissues or cell lines were collected using lysis buffer RIPA (1% deoxycholate, 1.5 mM MgCl₂, 50 mM HEPES, 0.1% sodium dodecyl sulfate, 1% Triton X-100, 150 mM NaCl, 10% glycerol, 1 mM EGTA, and protease inhibitor) (Bio-Rad). BCA protein reagent (Pierce) was used to measure protein concentration. Denaturing 10% SDS–polyacrylamide gel electrophoresis separated all samples which were then transferred to PVDF membrane. After blocked using TBST containing 5% milk for 1 h, indicated primary antibody was added on PVDF membranes at 4°C overnight. As previously described (Qu *et al*, 2016), secondary antibody was added and enhanced chemiluminescence (Pierce) were used to visualize blots.

Co-immunoprecipitation

As described (Qu *et al*, 2016), the indicated antibodies were added to the 500 µg of pre-cleared samples and were rotated at 4°C about 8 h. Then, A&G beads (Sigma) were mixed with samples for 3 h. Finally, the immunoprecipitation complexes were subjected to blot analysis.

Polymerase chain reaction

TRIzol (Thermo Fisher Scientific) was purchased to purify indicated RNA from GC cells or GC tissues. Then, random primers and a Reverse Transcription Kit (Invitrogen) were purchased to reversely transcribe total RNA into the complementary DNA (cDNA). Subsequently, RT–PCR was finished by Applied Biosystems. Primers for the respective genes were synthesized by Invitrogen. The relative levels of indicated proteins were analyzed through the 2^{−ΔΔCt} method. The endogenous control is GAPDH. All primer sequences are as follows: UHMK1, 5′-AGAGAAACCATGGCAGAAG-3′ and 5′-CAAGCCATGAAACAGCATCT-3′; ATF4, 5′-TTCTCCAGCGACAAGGCTAAGG-3′, 5′-CTCCAACATCCAATCTGTCCCG-3′; PPA1, 5′-GCGATTGAAGCACTGTG GATG-3′ and 5′-CGGTTTTTACACAGCACCTCC AC-3′; ADSL, 5′-TAGCGACAGGTATAAATTCC-3′ and 5′-TCTCCTGCCCTTGCTTTTCT-3′; GART, 5′-GGAATCCCAACCGCACAAATG-3′ and 5′-AGCAGGGAAGTCTGCACTCA-3′; IMPDH1, 5′-GTCTGCATCCCAACCAAAAG-3′ and 5′-ACTGCTGCAGGCCGGCTAC-3′; ATIC, 5′-CACGCTCGAGTGACAGTG-3′ and 5′-TCGGAGCTCTGCATCTCCG-3′; and GAPDH, 5′-GCCCAATACGACCAATCC-3′ and 5′-CACCACATCGCTCAGACAC-3′.

Metabolites assays

LC/MS/MS was used to analyze intracellular metabolites of indicated cells as described previously (Ben-Sahra *et al*, 2016). Briefly, glycine-free DMEM was used to wash indicated cells, and then, cells were added with the same medium containing 400 µM [13C1] for

30 min. For [15N]-glutamine (amide-labeled) flux studies, cells were washed once with glutamine-free DMEM and then incubated in the same medium containing 4 mM 15N-glutamine for 20 min. Metabolites were extracted using 4 ml 80% methanol on dry ice. After spinning at 4,000× g at 4°C, the insoluble pellets were isolated by 0.5 ml 80% methanol via spinning at 20,000× g at 4°C. An N-EVAP from Organomation Associates was used to dry the metabolites under nitrogen gas. The 10 µl HPLC grade water was added to resuspended pellets, and then, MS analysis was performed. Finally, AB/Sciex, a MultiQuant v2.0 software, was used to analyze the metabolite SRM transition. The SRMs were used to analyze the incorporation of 15N or 13C incorporation by LC-MS/MS.

Identifying UHMK1-binding proteins and NCOA3 phosphorylation sites by mass spectrometry

As described previously (Song *et al*, 2015), Flag-tagged UHMK1 was transfected into HEK293T cells, with an empty vector as control. Flag M2 agarose beads (Sigma) were used to pull down the proteins which bind to UHMK1 overnight. The washing buffer (0.2 mM PMSF, 15% glycerol, 1 mM EDTA, 0.05% Nonidet P (NP) 40, 1 mM dithiothreitol (DTT), 150 mM KCl, and 20 mM Tris–HCl) was made to rinse samples, and then, a TBS buffer followed. Finally, the eluted proteins were loaded on SDS–PAGE gels which were cut for MS analysis. NCOA3 phosphorylation sites were identified as described previously (Song *et al*, 2015).

Cell proliferation assay

Briefly, in normal medium, the Cell Counting Kit-8 (CCK-8) solution was added into GC cells in 10% dilution. Then, color conversion was observed. At indicated time points, proliferation rates of GC cells were examined after transfection.

Colony formation

Briefly, 500 indicated cells were seeded in the 6-well plate. After cultured at 37°C for about 2 weeks, 100% methanol was added into these cells. After discarding the methanol, sufficient trypan blue solution was added for staining. A digital camera was used to count the colonies. All experiments were repeated at least triplicate. The Mann–Whitney *U*-test was used for determining statistical significance.

Cell immigration and invasion assays

For invasion assays, Transwell with 8-µm pore and Matrigel (Corning Co.) were used to measure the invasive ability of GC cell lines. Briefly, indicated 2 × 10⁴ cells per well were seeded into the upper chamber after 48 h of transfection with 100 µl DMEM not containing FBS. Then, 500 µl medium was added to the lower chambers including 10% FBS which acted as a chemoattractant. Twenty-four hours later, wipe off cells left on the upper membrane with a cotton swab while keeping the cells that had invaded. After fixed in 4% formaldehyde, 1% crystal violet was used to stain the invaded cells. An inverted microscope (Nikon) was used to count ten random visual fields. For migration assay, Transwell with 8-µm pore insert without Matrigel was used. Similar way to invasion assay was used.

GST pull-down assay

As previously described (Song *et al*, 2015), *Escherichia coli* was used to express GST-fusion proteins. Then, IPTG induced their expression. Proteins were purified using glutathione Sepharose 4B beads purchased from Sigma. GST-tagged UHMK1 or NCOA3, and GST (around 10 μ g) were cross-linked by dimethyl pimelimidate dihydrochloride to glutathione Sepharose in reaction buffer (10% glycerol, 1 mM EDTA, 20 mM HEPES; 150 mM KCl, 0.1% Nonidet P (NP) 40), pH 8.0. After eluted with sample buffer, Coomassie staining and Western blot were used to analyze the samples.

Luciferase reporter assays

As described previously (Hong *et al*, 2014), we cultured HEK293T cells to perform the dual-luciferase reporter assays. Briefly, using Lipofectamine 2000 overnight after plating, 0.2 μ g of the firefly promoter–luciferase reporter constructs (WT-UHMK1 or UHMK1 mutant promoter) was co-transfected with indicated plasmids. The control group was PGL-TK Renilla luciferase plasmid. The activity was monitored via a Dual-Luciferase System bought from Promega. And the luciferase activity was averaged from three replicates.

Chromatin immunoprecipitation (ChIP)

As described (Qu *et al*, 2016), the primers which were adopted for ATF4 motif are, respectively, (5'-CTGTATCTTGTTGAC-3') and (5'-GGAAATGCAGCCAGTA-3'); (5'-CTTAGATAAGAATTTGG-3') and (5'-GTAATCCAGCACTTTG-3').

Mice xenograft experiments

In accordance with NIH Guidelines, mice experiments were performed. And the Institutional Animal Committee at Harbin Medical University approved animal protocols. For xenograft model, BGC823-pLV-UHMK1 and BGC823-pLV-NC or SGC7901-pLV-shUHMK1 or SGC7901-pLV-shcontrol were bought and implanted into the posterior flank of the nude mouse ($n = 10$ /group). At indicated time, the size and volume of the tumor were calculated as described previously (Hong *et al*, 2014).

Tissue arrays and immunohistochemical (IHC) staining

GC tissue microarray (TMA) was purchased from Alenabio Company, and IHC staining was performed for UHMK1. As described previously (Qu *et al*, 2016), IHC staining was evaluated and scored by the scale: 0, 1+, 2+, and 3+, representing no staining, weak, moderate, and strong staining, respectively. The final H-score was calculated based on the formula reported previously (Hirsch *et al*, 2003). The indicated protein levels were defined by H-score; then, low and high expression patient groups were divided.

Immunoprecipitation kinase analysis

As described before (Prieto-Echagüe *et al*, 2010), IP kinase assay was done. Briefly, the lysate (1 mg) was mixed with anti-HA antibody (Santa Cruz). Twenty-four hours later, protein G-agarose

beads (Santa Cruz) were added. The immunocomplexes were resuspended in buffer containing 1 mM Na_3VO_4 . By using the phosphocellulose paper assay, the immunoprecipitated UHMK1 activity was examined as follows. One synthetic peptide (1 mM) derived from the CATS protein phosphorylation site (a known substrate of UHMK1) was added as a substrate in the mixture (0.4 mM ATP, 10 mM MgCl_2 , 1 mM Na_3VO_4 , 20 mM Tris, and $[\gamma\text{-}^{32}\text{P}]\text{ATP}$ pH 7.4. After 30 min at 30°C, 10% trichloroacetic acid terminated the reaction. Then, the mixtures were loaded as a dot on the p81 phosphocellulose paper. Scintillation counting was used to determinate incorporation of ^{32}P into peptide.

TCGA and oncomine data

Whole-genome RNA sequencing (RNA-seq) data about the gastric cancer TCGA dataset were downloaded by website: <https://xenabrowser.net>. The patients with unavailable survival data were excluded. The relevant clinical characteristics, including age, gender, pathologic TNM, disease stage, survival time, and censor, were obtained from TCGA dataset. Samples in three groups were stratified according to their UHMK1 gene levels (low, intermediate, high). The 25th and 75th percentiles were used as cutoff. Benjamini–Hochberg procedure was used to calculate the false discovery rate and top 500 upregulated genes were chosen for gene ontology analysis by <https://biit.cs.ut.ee/gprofiler/gost>.

A web-based data mining platform and cancer microarray database, Oncomine data about UHMK1 analysis in GC were also downloaded from the public websites. The expression pattern was plotted using GraphPad Prism 7 software.

GC metastasis model

For GC metastasis assays, the abdominal cavities of 4- to 6-week-old male BALB/c nu/nu were injected with about 1×10^6 cells with BGC823-pLV-UHMK1 or BGC823-pLV-NC or SGC7901-pLV-shUHMK1 or SGC7901-pLV-shcontrol. At indicated times, peritoneal metastatic tumors were counted, imaged, and presented.

In vitro kinase

1 μ g recombinant UHMK1 protein and purified WT-NCOA3 or its mutant proteins were mixed with $1 \times$ reaction buffer containing 10 μ M ATP and 0.2 mM Na_3VO_4 and 10 μ Ci $[\gamma\text{-}^{32}\text{P}]\text{ATP}$. The reaction proceeded at 30°C for 15 min. Then, the mixtures were separated and incorporated $[\gamma\text{-}^{32}\text{P}]$ radioisotope was detected by imaging plate-autoradiography system.

Infection of cell lines or mice with *H. pylori*

The *Cag*⁺ *H. pylori* strains used in this project were as followed: wild-type (WT) 7.13, J166, and PMSS1 which is a rodent-adapted bacteria. As previously described (Zhu *et al*, 2017), for passage *in vitro*, trypticase soy agar plates were used to culture these strains with 5% sheep blood (Invitrogen). Then, at 37°C with 5% CO_2 , Brucella broth (Invitrogen) was used to culture *H. pylori* bacteria with 10% FBS (Sigma) about 18 h. For *in vitro* studies, gastric epithelial cells were infected with *H. pylori* strains by using a multiplicity of infection (MOI) of 50:1.

For mice, Brucella broth orogastrically challenged C57BL/6 mice ($n = 10/\text{group}$) with or without WT PMSS1 *H. pylori* bacteria (10^9 CFU per mouse). About 8 weeks later postchallenge, all mice were euthanized. Then, whole gastric tissues were collected, and real-time polymerase chain reaction (PCR) and immunoblots were performed (Noto *et al*, 2013).

Statistics

The Student's *t*-test was used to analyze the results from two groups. As comparing data from the groups greater than two, we used one-way ANOVA. To analyze the growth curves, we used two-way ANOVA. Pearson's correlation analysis was used to elucidate the correlation of two proteins. Program for GraphPad Prism 5, R software package (version 3.0.0), and Social Sciences software 20.0 (SPSS) was used. Determining Kaplan–Meier data needed the log-rank test. Data were reported through mean \pm SD, at least carried out in triplicate. Statistical value ($*P < 0.05$) was significant. $**P < 0.01$ or $***P < 0.001$ was very significant, while # marked no significance.

Data availability

The mass spectrometry raw data included from this publication have been deposited to the ProteomeXchange Consortium (<http://www.proteomexchange.org/>) via the PRIDE partner repository and assigned the identifier PRIDE: PXD015693.

Expanded View for this article is available online.

Acknowledgements

The authors would like to thank the Cancer Institute of New Jersey for providing the supports of the entire research team. This work was supported by National Natural Science Foundation of China (No. 81702387, No. 81702744), Natural Science Foundation of Fujian Province (No. 2017J01368, No. 2017J01369), Training Program for Young Talents of Fujian Health System (No. 2016-ZQN-85), Fujian Provincial Funds for Distinguished Young Scientists (No. 2018D0016), and Fujian Health Education Joint Research Project (WKJ2016-2-17). The funders had no role in study design, data collection and analysis, decision to publish, or preparation of the manuscript. The authors also thank Shanghai Tongshu Biotechnology Co., Ltd. for technical support.

Author contributions

XF and XH designed and evaluated the concept of this study; XF, DM, JZ, YS, YZ, QZ, FM, XL, MZ, YL, YX, XQ, and KZ acquired data; ZZ, FM, HZ, YZ, and XL analyzed and interpreted data; XF, XH, and ZZ drafted the manuscript, which was critiqued by all authors; ZZ was responsible for study supervision of the study and critical revision of the manuscript for important intellectual content.

Conflict of interest

The authors declare that they have no conflict of interest.

References

Barbutti I, Machado-Neto JA, Arfelli VC, de Melo Campos P, Traina F, Olalla Saad ST, Froehlich Archangelo L (2017) The U2AF homology motif kinase 1

- (UHMK1) is upregulated upon hematopoietic cell differentiation. *Biochim Biophys Acta Mol Basis Dis* 1864: 959–966
- Ben-Sahra I, Hoxhaj G, Ricoult SJH, Asara JM, Manning BD (2016) mTORC1 induces purine synthesis through control of the mitochondrial tetrahydrofolate cycle. *Science* 351: 728–733
- Boehm M, Yoshimoto T, Crook MF, Nallamshetty S, True A, Nabel GJ, Nabel EG (2002) A growth factor-dependent nuclear kinase phosphorylates p27Kip1 and regulates cell cycle progression. *EMBO J* 21: 3390–3401
- Bouzar AB, Boxus M, Defoiche J, Berchem G, Macallan D, Pettengell R, Willis F, Burny A, Lagneau L, Bron D *et al* (2009) Valproate synergizes with purine nucleoside analogues to induce apoptosis of B-chronic lymphocytic leukaemia cells. *Br J Haematol* 144: 41–52
- Burton C, Ma Y (2019) Current trends in cancer biomarker discovery using urinary metabolomics: achievements and new challenges. *Curr Med Chem* 26: 5–28
- Cambray S, Pedraza N, Rafel M, Gari E, Aldea M, Gallego C (2009) Protein kinase KIS localizes to RNA granules and enhances local translation. *Mol Cell Biol* 29: 726–735
- Dasgupta S, Rajapakse K, Zhu B, Nikolai BC, Yi P, Putluri N, Choi JM, Jung SY, Coarfa C, Westbrook TF *et al* (2018) Metabolic enzyme PFKFB4 activates transcriptional coactivator SRC-3 to drive breast cancer. *Nature* 556: 249–254
- Dayie TK, Thakur CS (2010) Site-specific labeling of nucleotides for making RNA for high resolution NMR studies using an *E. coli* strain disabled in the oxidative pentose phosphate pathway. *J Biomol NMR* 47: 19–31
- Diaz P, Valenzuela Valderrama M, Bravo J, Quest AFG (2018) *Helicobacter pylori* and gastric cancer: adaptive cellular mechanisms involved in disease progression. *Front Microbiol* 9: 5
- Francone VP, Ifrim MF, Rajagopal C, Leddy CJ, Wang Y, Carson JH, Mains RE, Eipper BA (2010) Signaling from the secretory granule to the nucleus: Uhmk1 and PAM. *Mol Endocrinol* 24: 1543–1558
- Grant RC, Denroche RE, Borgida A, Virtanen C, Cook N, Smith AL, Connor AA, Wilson JM, Peterson G, Roberts NJ *et al* (2018) Exome-wide association study of pancreatic cancer risk. *Gastroenterology* 154: 719–722 e3
- Gupta A, Hossain MM, Miller N, Kerin M, Callagy G, Gupta S (2016) NCOA3 coactivator is a transcriptional target of XBP1 and regulates PERK-eIF2alpha-CDK1 signalling in breast cancer. *Oncogene* 35: 5860–5871
- Hirsch FR, Varella-Garcia M, Bunn PA Jr, Di Maria MV, Veve R, Bremmes RM, Barón AE, Zeng C, Franklin WA (2003) Epidermal growth factor receptor in non-small-cell lung carcinomas: correlation between gene copy number and protein expression and impact on prognosis. *J Clin Oncol* 21: 3798–3807
- Hong X, Song R, Song H, Zheng T, Wang J, Liang Y, Qi S, Lu Z, Song X, Jiang H *et al* (2014) PTEN antagonises Tc1/hnRNP-mediated G6PD pre-mRNA splicing which contributes to hepatocarcinogenesis. *Gut* 63: 1635–1647
- Hong X, Huang H, Qiu X, Ding Z, Feng X, Zhu Y, Zhuo H, Hou J, Zhao J, Cai W *et al* (2018) Targeting posttranslational modifications of RIOK1 inhibits the progression of colorectal and gastric cancers. *Elife* 7: e29511
- Karigane D, Kobayashi H, Morikawa T, Ootomo Y, Sakai M, Nagamatsu G, Kubota Y, Goda N, Matsumoto M, Nishimura EK *et al* (2016) p38alpha activates purine metabolism to initiate hematopoietic stem/progenitor cell cycling in response to stress. *Cell Stem Cell* 19: 192–204
- Katchman BA, Chowell D, Wallstrom G, Vitonis AF, LaBaer J, Cramer DW, Anderson KS (2017) Autoantibody biomarkers for the detection of serous ovarian cancer. *Gynecol Oncol* 146: 129–136
- Li J, Poulidakos PI, Dai Z, Testa JR, Callaway DJ, Bu Z (2007) Protein kinase C phosphorylation disrupts Na⁺/H⁺ exchanger regulatory factor 1

- autoinhibition and promotes cystic fibrosis transmembrane conductance regulator macromolecular assembly. *J Biol Chem* 282: 27086–27099
- Li B, Li H, Bai Y, Kirschner-Schwabe R, Yang JJ, Chen Y, Lu G, Tzoneva G, Ma X, Wu T et al (2015) Negative feedback-defective PRPS1 mutants drive thiopurine resistance in relapsed childhood ALL. *Nat Med* 21: 563–571
- Ma F, Zhu Y, Liu X, Zhou Q, Hong X, Qu C, Feng X, Zhang Y, Ding Q, Zhao J et al (2019) Dyrk3 loss activates the purine metabolism and promotes hepatocellular carcinoma progression. *Hepatology* 70: 1785–1803
- Manceau V, Kielkopf CL, Sobel A, Maucuer A (2008) Different requirements of the kinase and UHM domains of KIS for its nuclear localization and binding to splicing factors. *J Mol Biol* 381: 748–762
- Matsuoka T, Yashiro M (2014) The role of PI3K/Akt/mTOR signaling in gastric carcinoma. *Cancers* 6: 1441–1463
- Nishimura T, Nakata A, Chen X, Nishi K, Meguro-Horike M, Sasaki S, Kita K, Horike SI, Saitoh K, Kato K et al (2019) Cancer stem-like properties and gefitinib resistance are dependent on purine synthetic metabolism mediated by the mitochondrial enzyme MTHFD2. *Oncogene* 38: 2464–2481
- Noto JM, Khizanishvili T, Chaturvedi R, Piazuelo MB, Romero-Gallo J, Delgado AG, Khurana SS, Sierra JC, Krishna US, Suarez G et al (2013) *Helicobacter pylori* promotes the expression of Kruppel-like factor 5, a mediator of carcinogenesis, in vitro and in vivo. *PLoS ONE* 8: e54344
- Noto JM, Rose KL, Hachey AJ, Delgado AG, Romero-Gallo J, Wroblewski LE, Schneider BG, Shah SC, Cover TL, Wilson KT et al (2019) Carcinogenic *Helicobacter pylori* strains selectively dysregulate the *in vivo* gastric proteome, which may be associated with stomach cancer progression. *Mol Cell Proteomics* 18: 352–371
- Prieto-Echagüe V, Gucwa A, Craddock BP, Brown DA, Miller WT (2010) Cancer-associated mutations activate the nonreceptor tyrosine kinase Ack1. *J Biol Chem* 285: 10605–10615
- Qu C, He L, Dong L, Zhu Y, Zhao Q, Jiang X, Chang P, Jiang X, Wang L, Zhang Y et al (2016) Salt-inducible Kinase (SIK1) regulates HCC progression and WNT/beta-catenin activation. *J Hepatol* 64: 1076–1089
- Selvarajah B, Azuelos I, Platé M, Guillotin D, Forty EJ, Contento G, Woodcock HV, Redding M, Taylor A, Brunori G et al (2019) mTORC1 amplifies the ATF4-dependent de novo serine-glycine pathway to supply glycine during TGF- β_1 -induced collagen biosynthesis. *Sci Signal* 12: eaav3048
- Song R, Song H, Liang Y, Yin D, Zhang H, Zheng T, Wang J, Lu Z, Song X, Pei T et al (2014) Reciprocal activation between ATPase inhibitory factor 1 and NF-kappaB drives hepatocellular carcinoma angiogenesis and metastasis. *Hepatology* 60: 1659–1673
- Song H, Pu J, Wang L, Wu L, Xiao J, Liu Q, Chen J, Zhang M, Liu Y, Ni M et al (2015) ATG16L1 phosphorylation is oppositely regulated by CSNK2/casein kinase 2 and PPP1/protein phosphatase 1 which determines the fate of cardiomyocytes during hypoxia/reoxygenation. *Autophagy* 11: 1308–1325
- Song H, Feng X, Zhang M, Jin X, Xu X, Wang L, Ding X, Luo Y, Lin F, Wu Q et al (2018) Crosstalk between lysine methylation and phosphorylation of ATG16L1 dictates the apoptosis of hypoxia/reoxygenation-induced cardiomyocytes. *Autophagy* 14: 825–844
- Soutto M, Chen Z, Katsha AM, Romero-Gallo J, Krishna US, Piazuelo MB, Washington MK, Peek RM Jr, Belkhiri A, El-Rifai WM (2015) Trefoil factor 1 expression suppresses *Helicobacter pylori*-induced inflammation in gastric carcinogenesis. *Cancer* 121: 4348–4358
- Sullivan LB, Gui DY, Vander Heiden MG (2016) Altered metabolite levels in cancer: implications for tumour biology and cancer therapy. *Nat Rev Cancer* 16: 680–693
- Wang H, Zhan M, Yang R, Shi Y, Liu Q, Wang J (2018) Elevated expression of NFE2L3 predicts the poor prognosis of pancreatic cancer patients. *Cell Cycle* 17: 2164–2174
- Wroblewski LE, Peek RM Jr, Wilson KT (2010) *Helicobacter pylori* and gastric cancer: factors that modulate disease risk. *Clin Microbiol Rev* 23: 713–739
- Yoshizawa T, Hinoi E, Jung DY, Kajimura D, Ferron M, Seo J, Graff JM, Kim JK, Karsenty G (2009) The transcription factor ATF4 regulates glucose metabolism in mice through its expression in osteoblasts. *J Clin Invest* 119: 2807–2817
- Yusefi AR, Bagheri Lankarani K, Bastani P, Radinmanesh M, Kavosi Z (2018) Risk factors for gastric cancer: a systematic review. *Asian Pac J Cancer Prev* 19: 591–603
- Zhu S, Soutto M, Chen Z, Peng D, Romero-Gallo J, Krishna US, Belkhiri A, Washington MK, Peek R, El-Rifai W (2017) *Helicobacter pylori*-induced cell death is counteracted by NF-kappaB-mediated transcription of DARPP-32. *Gut* 66: 761–762
- Zhu Y, Qu C, Hong X, Jia Y, Lin M, Luo Y, Lin F, Xie X, Xie X, Huang J et al (2019) Trabid inhibits hepatocellular carcinoma growth and metastasis by cleaving RNF8-induced K63 ubiquitination of Twist1. *Cell Death Differ* 26: 306–320